OFFICE OF NAVAL RESEARCH

Contract N00014-82-K-0280

Task No. NR413E001

TECHNICAL REPORT NO. 20

The Adsorption and Decomposition of NH_3 on Si(100) - Detection of the NH_2(a) Species

by

M. J. Dresser, P. A. Taylor, R. M. Wallace, W. J. Choyke,

and J. T. Yates, Jr.

Prepared for Publication in

Surface Science

Surface Science Center
Department of Chemistry
University of Pittsburgh
Pittsburgh, PA 15260

6 December 1988

UNCLASSIFIED
SECURITY CLASSIFICATION OF THIS PAGE (When Data Entered)

MASTER COPY - FOR REPRODUCTION PURPOSES

REPORT DOCUMENTATION PAGE		READ INSTRUCTIONS BEFORE COMPLETING FORM
1. REPORT NUMBER 20	2. GOVT ACCESSION NO.	3. RECIPIENT'S CATALOG NUMBER
4. TITLE (and Subtitle) The Adsorption and Decomposition of NH_3 on Si(100) - Detection of the NH_2(a) species		5. TYPE OF REPORT & PERIOD COVERED 6. PERFORMING ORG. REPORT NUMBER
7. AUTHOR(s) M.J. Dresser, P.A. Taylor, R.M. Wallace, W.J. Choyke, and J. T. Yates, Jr.		8. CONTRACT OR GRANT NUMBER(s) N00014-82-k-0280
9. PERFORMING ORGANIZATION NAME AND ADDRESS Surface Science Center, Chemistry Dept. University of Pittsburgh, Pittsburgh, PA 15260		10. PROGRAM ELEMENT, PROJECT, TASK AREA & WORK UNIT NUMBERS
11. CONTROLLING OFFICE NAME AND ADDRESS		12. REPORT DATE 12/14/88 13. NUMBER OF PAGES
14. MONITORING AGENCY NAME & ADDRESS(if different from Controlling Office)		15. SECURITY CLASS. (of this report) Unclassified 15a. DECLASSIFICATION/DOWNGRADING SCHEDULE

16. DISTRIBUTION STATEMENT (of this Report)

17. DISTRIBUTION STATEMENT (of the abstract entered in Block 20, if different from Report)

18. SUPPLEMENTARY NOTES

19. KEY WORDS (Continue on reverse side if necessary and identify by block number)

ammonia, Si(100), silicon nitride, ESDIAD, amino species, NH_2

20. ABSTRACT (Continue on reverse side if necessary and identify by block number)

The dissociative adsorption of NH_3 on Si(100)(2x1) has been studied using accurate surface coverage measurements, temperature programmed desorption, Auger spectroscopy and digital ESDIAD/LEED methods. It has been found that NH_2 surface species (amino species) are produced to a saturation coverage of 1 NH_2/Si dimer at 120 K. This is accompanied by the production of a Si-H surface species. Digital ESDIAD measurements of the H^+ angular distribution from NH_2(a) species indicate that torsional oscillations about the Si-NH_2 bond are responsible for the characteristic elliptical H^+ pattern whose long axis is perpendicular to the Si-Si dimer bond direction. It has been shown that NH_3 dissociatively adsorbs with unity sticking probability at 120 K up to 86% of full coverage, indicative of a mobile precursor adsorption mechanism. The pre-adsorption of atomic H onto the Si dangling bond sites reduces the adsorptive capacity of the Si(100) surface, and 1 H/Si completely passivates the surface for NH_3 chemisorption. The NH_2(a) species,

DD FORM 1 JAN 73 1473 EDITION OF 1 NOV 65 IS OBSOLETE

UNCLASSIFIED
SECURITY CLASSIFICATION OF THIS PAGE (When Data Entered)

20. produced by adsorption at 120 K are stable up to about 600 K, where decomposition occurs to produce N(a) and H(a). A minor reaction channel involving NH_2(a) + H(a) to produce recombined NH_3(g) is observed in the temperature range 600 - 700 K. Above 700 K, surface N(a), produced from NH_2(a) decomposition, enters into the Si(100) lattice.

Submitted: Surface Science

Date: 2 December 1988

THE ADSORPTION AND DECOMPOSITION OF NH_3 ON Si(100) - DETECTION OF THE NH_2(a) SPECIES.

M.J. Dresser[‡], P.A. Taylor, R.M. Wallace, W.J. Choyke[‡‡] and J.T. Yates, Jr.[†]

Surface Science Center
Department of Chemistry
University of Pittsburgh
Pittsburgh, PA 15260

[†]Author to whom correspondence should be addressed

[‡]Permanent address: Department of Physics, Washington State University, Pullman, Washington 99164-2814

[‡‡]Department of Physics, University of Pittsburgh, Pittsburgh, PA 15260

THE ADSORPTION AND DECOMPOSITION OF NH_3 ON Si(100) - DETECTION OF THE NH_2(a) SPECIES.

M.J. Dresser[‡], P.A. Taylor, R.M. Wallace, W.J. Choyke[‡‡] and J.T. Yates, Jr.

Surface Science Center
Department of Chemistry
University of Pittsburgh
Pittsburgh, PA 15260

Abstract

The dissociative adsorption of NH_3 on Si(100)(2x1) has been studied using accurate surface coverage measurements, temperature programmed desorption, Auger spectroscopy and digital ESDIAD/LEED methods. It has been found that NH_2 surface species (amino species) are produced to a saturation coverage of 1 NH_2/Si dimer at 120 K. This is accompanied by the production of a Si-H surface species. Digital ESDIAD measurements of the H^+ angular distribution from NH_2(a) species indicate that torsional oscillations about the Si-NH_2 bond are responsible for the characteristic elliptical H^+ pattern whose long axis is perpendicular to the Si-Si dimer bond direction. It has been shown that NH_3 dissociatively adsorbs with unity sticking probability at 120 K up to 86% of full coverage, indicative of a mobile precursor adsorption mechanism. The preadsorption of atomic H onto the Si dangling bond sites reduces the adsorptive capacity of the Si(100) surface, and 1 H/Si completely passivates the surface for NH_3 chemisorption. The NH_2(a) species, produced by adsorption at 120 K are stable up to about 600 K, where decomposition occurs to produce N(a) and H(a). A minor reaction channel involving NH_2(a) + H(a) to produce recombined NH_3(g) is observed in the temperature range 600 - 700 K. Above 700 K, surface N(a), produced from NH_2(a) decomposition, enters into the Si(100) lattice.

I. INTRODUCTION

The adsorption and thermal decomposition of molecules on Si single crystal surfaces is of current interest for several reasons. First, information about this type of surface chemistry is of importance in semiconductor technology where adsorption followed by thermal decomposition is one mode of controlled thin film growth [1]. Secondly, the investigation of the chemistry of the "dangling bond" electronic states present at the surface of covalently-bound solids is of major fundamental interest in comparison to surface chemistry on metals where more delocalized surface electronic states are present [2-4]. Thirdly, with the advent of atomic level imaging techniques such as the scanning tunnelling microscope (STM), which is so effective on covalent solid surfaces, it is of current importance to bring other surface measurement techniques to bear upon the same systems in order to achieve a more complete understanding of the chemistry which occurs in these systems, as well as greater understanding of the meaning of the STM images [3,4].

The adsorption of NH_3 on Si(100) is a prototype chemical system for the achievement of the three objectives listed above. NH_3 is an important molecule for producing silicon nitride films by both thermal and electronically-excited silicon nitride thin film growth processes [5,6]. The chemistry of NH_3 on transition metals is fairly well understood [7], and comparisons with its chemistry on Si single crystals can therefore be made. Finally, a wide variety of surface measurement techniques have been applied to the study of NH_3 interaction and thermal decomposition on Si(100) and Si(111). These techniques include STM [3,4,8,9], XPS [3-6,10-13], UPS [3,4,6,9,10,14,15], HREELS [11,16,17], ISS [3,5], TPD [3,5], laser vaporization/FTMS [18] and one ESDIAD study [19].

A controversy exists concerning whether NH_3 adsorbs dissociatively at temperatures near 100 K on Si single crystal surfaces. This paper addresses this question, and also identifies the primary stable surface species produced from NH_3 dissociative adsorption. On Si(100), Avouris et al [3] report that even at 90 K, NH_3 is dissociated to adsorbed H and adsorbed N. The adsorbed N was reported to penetrate into the subsurface region of Si(100) where silicon nitride is produced at low temperatures. In contrast to this, Hlil et al [10], using both UPS and XPS methods, have reported that NH_3 adsorbed at 100 K on Si(100) is present as an undissociated molecule. This view is based upon the observation of the characteristic $3a_1$ (N lone pair electrons) and the 1e (N-H bonding electrons) UPS features at 100 K on both Si(100) and Si(111). Near 300 K the UPS spectrum changes slightly and these two orbitals shift by about 1.0 eV and 0.7 eV to lower binding energy as an Si-H UPS feature develops. This general view of NH_3 dissociation at about 300 K is verified by XPS studies of the N(1s) level for various surface temperatures. Between 100 K and 300 K, adsorbed NH_3 is postulated to convert to adsorbed NH_x as seen by a 1.5 eV shift to lower N(1s) binding energy. Silicon nitride formation is observed above 590 K, as the N(1s) binding energy shifts a total of 2.6 eV to lower N(1s) binding energy compared to that for NH_3(a) [10]. Tanaka, et al [16] have studied the adsorption of NH_3 by Si(111) using HREELS. They report that the Si(111)-(7 x 7) surface adsorbs NH_3 at 300 K to produce a mixture of $Si-NH_2$ and Si-NH species. Upon heating to 700 K, $Si-NH_2$ species are partially decomposed to form Si_3N_4 and Si-H surface species. At 900 K all H atoms are removed from the surface. Kilday et al [11], using HREELS and XPS, conclude that Si(111) adsorbs NH_3 molecularly at 300 K, with some dissociation taking place as seen by the presence of an Si-H

stretching frequency at 2055 cm^{-1}. Johnson et al [19], using ESDIAD, conclude that NH_x species are produced at 0.1 L [1 L = 1 Langmuir = 1 x 10^{-6} Torr sec] exposure at 125 K on Si(100); these species are reported to produce 2 H^+ ESDIAD beams which are observed to be directed perpendicular to the Si-Si dimer axes. This behavior was likened to that observed for adsorbed -OH species on the dimerized Si(100) surface. At a 2.0 L NH_3 exposure at 125 K, only a broad normally-directed H^+ ESDIAD beam could be detected.

Recently Avouris et al [4,6], as a refinement of their earlier findings [3], have reported that Si(100)-(2x1) dissociates NH_3 at 100 K to produce NH surface species. The tentative assignment of the species as NH(a) rather than NH_2(a) or NH_3(a) was based on small differences between the N(1s) XPS spectrum of the species on Si(100)-(2x1) and Si(111)-(7x7), where NH_2 was the preferred assignment on Si(111)-(7x7). In addition, UPS studies were interpreted to indicate that Si(100) is more reactive toward NH_3 than is Si(111).

The investigation reported here has been carried out using a combination of methods appropriate to this problem. We will show that the production of NH_2 species from NH_3(g) can be observed on the Si(100)-(2x1) surface using digital ESDIAD. In addition, the recombination of NH_2(a) species with H(a) has been observed above 550 K, and studies of isotopic exchange of D(a) into the NH_2(a) species confirm that it is in fact NH_2(a).

II. EXPERIMENTAL

A. General Description of the Apparatus

A top view of the ultrahigh vacuum apparatus (base pressure = 5 x 10^{-11} Torr) used in this work is shown in Figure 1. The apparatus is

pumped by a 200 L/s triode ion pump, a 150 L/s turbo pump, and a titanium sublimation pump. We estimate the pumping time constant of the system to be 0.5 sec. A Si single crystal of approximate square geometry is mounted on the end of a cooled support assembly which can be rotated 360° to allow the crystal to face various measurement instruments in the bell jar. A LEED/ESDIAD analyzer which involves resistive anode detection and digital data acquisition facilities is located at the bottom of the figure [20,21]. In addition, a digitally multiplexed quadrupole mass spectrometer (QMS) (which samples 1-6 masses/second) is located so that the crystal may be positioned directly on axis for temperature programmed desorption measurements, as well as for measurements of the kinetics of adsorption when gas impinges on the crystal surface from a collimated and calibrated directed beam doser [22]. The collimation of the beam is achieved by the use of a glass microcapillary array located at the front of the doser [22], and the fraction of the beam intercepted by the crystal may be determined by direct measurement or estimated from the geometry of the apparatus [23,24]. For studies of the identity of the ionic species produced by ESD, an electron gun identical to that used in the digital LEED/ESDIAD measurements, located near the QMS, may be used to irradiate the crystal. The positive ions are accelerated into the QMS (internal ionization source off) through a pair of planar grids biased such that ions arrive at the QMS with 40 eV kinetic energy; scattered electrons are retarded. Atomic hydrogen (deuterium) is produced from H_2 (D_2) gas ($\sim 1 \times 10^{-8}$ Torr = $P_{H_2(D_2)}$) using a tungsten spiral filament which operates at 1800 K. Auger spectroscopy of the Si(100) surface may be carried out using a Varian scanning Auger cylindrical mirror analyzer. The crystal may be ion bom-

barded for cleaning using a rastered ion gun which directs an Ar^+ beam on the crystal at an angle of incidence of 70° with respect to the surface normal. Normally the Ar^+ current is 4×10^{-6} A and the bombardment energy is 2 KeV.

A more detailed view of the digital LEED/ESDIAD apparatus is shown in Figure 2. An electron gun (Comstock EG-401) modified with x and y deflection plates delivers an electron beam at an angle of incidence of 50° to the silicon single crystal. For all measurements in this paper, the Si crystal is biased at + 10 V causing some ESDIAD pattern compression effects. Thus, all angles of ion emission are closer to the normal than would be observed without compression effects. Because of the low dielectric constant of the silicon substrate, image charge effects, which would cause the polar angles to be larger, should be minimal. At lower compression voltages, H^+ ions are not collected efficiently in the ESDIAD apparatus. Calculations indicate and direct observations show that, for a crystal bias greater than +30 V, further compression of the ion patterns is minor.

For ESDIAD measurements, the electron beam (5×10^{-9} A, 210 eV) used to excite a spot on the crystal is 1 mm in diameter. Positive ions produced by the ESDIAD process are intercepted by 3 concentric hemispherical grids (G_1 - G_3, numbered in order of distance from the crystal) which are operated at the following bias voltages ($G_1 = G_2 =$ 0V; $G_3 = +5$ V); the positive ions then pass through a planar grid ($G_4 =$ -350 V). The ions then exit to the microchannel plate assembly through a drift zone of length 4.5 cm. The microchannel plate input potential is typically -400 V, and a potential drop of 880 V is applied across each microchannel plate. The pulsed electron output of the microchannel

plates, amplified by a factor of about 10^5, is collected by a two-dimensional resistive anode (Surface Science Laboratories, model 3394A), and fed into the computerized data collection and manipulation system which has been described previously [20,21]. Typical ion counting times are 120 s, and a typical digital ESDIAD pattern contains about 2×10^6 ion counts. This detection system has the advantage of high sensitivity for low signals and only an 8 s maximum time between data acquisition and full graphic display. It was found that the provision of internal shielding was necessary in the region of the ESDIAD grids and the drift zone; these shields were operated at the planar grid and microchannel plate input potentials, respectively.

For digital LEED measurements, the potentials in the grid system are reversed (G_1 = 0 V, $G_2 = G_3$ = -60 V, G_4 = -95 V). The electron beam ($< 1 \times 10^{-9}$ A, 100 V) is provided by the same gun as in the digital ESDIAD measurements. Because of the length of the drift zone, our LEED beams are broader than those normally measured in conventional digital LEED systems [20,21].

B. Auger Measurements

The effect of electron beam-enhanced chemistry has been shown to be important for silicon carbide and silicon nitride film growth resulting from the reaction of the Si(100) surface with hydrocarbons and NH_3 [25,3,5]. When careful AES measurements are to be made, the issue of electron beam damage of the adsorbate during the acquisition of an Auger electron spectrum must be addressed.

The integral electron gun used in the CMA produces a spot of 0.2 mm diameter at a focal length of 2 cm. The 3 keV electron beam current is

typically 2 x 10^{-6} A during the analysis. These parameters result in an electron flux of 4 x 10^{16} $s^{-1}cm^{-2}$, which is certainly large enough to produce the dissociation of NH_3 adsorbate on the surface when scan times of ~ 120 seconds are considered. We therefore use the Auger measurements as a relative assay of the nitride species produced by electron beam degradation from NH_2 surface species present before thermal decomposition. The nitride Auger signal is proportional to the nitrogen coverage present from the NH_2 surface species, as shown by measurements of the N Auger intensity increase with increasing NH_3 coverage.

All of the Auger data reported herein are the result of a four point average over the exposed surface of the crystal. With a 0.2 mm electron beam diameter, a total area of 0.0012 cm^2 is exposed to the focused electron beam, which represents only 0.06% of the available surface area. We can therefore conclude that AES and TPD measurements may be safely carried out together without the production of spurious effects in TPD measurements due to electron beam degradation of an appreciable fraction of the adsorbed layer.

C. Calibration of the Beam Doser

In the measurements reported here, it was of importance to determine as accurately as possible the incident flux of adsorbate on the single crystal. The collimated directed beam doser allows this to be done. A measurement of the delivery rate of the doser for NH_3 was carried out using accurate methods as described below. A Baratron capacitance manometer (0 - 10 Torr, precision = 0.001 Torr) was used to measure the pressure drop in the stainless steel gas handling system of known volume (209.2 cm^3) over a period of about 1.8 x 10^5 s., as shown

in Figure 3. The slope of the semilogarithmic plot may be used to accurately determine the conductance of the nominal 2 micron conductance-limiting orifice located in the delivery tube of the doser [22]. At 1.040 Torr NH_3 pressure, the measured conductance is 3.68 (±.03) x 10^{13} NH_3 molecules/s at 299.5 ± 0.9 K. The reasons for the first two points in this measurement being high may have to do with slow adsorption effects on the walls of the doser gas handling system, and these points are not included in the analysis. The measurement in Figure 3, combined with various estimates of the fraction of the NH_3 beam intercepted by the crystal [23,24] may be used to compute the flux of NH_3 incident per unit area on the crystal. A careful propagation of errors analysis has yielded a maximum uncertainty of 30% for absolute exposure and coverage measurements with this dosing apparatus, although our precision is much better as revealed by good reproducibility of Auger and TPD measurements as a function of NH_3 exposure.

D. Preparation, Mounting and Cleaning of the Si(100) Crystal

The (15 mm x 17 mm x 1.5 mm; 2.6 cm^2 area) Si(100)(10 ohm-cm) crystal (orientation accuracy = 1°) was slotted on all four edges with a diamond saw to produce 0.4 mm slots of 1.5 mm depth. Two of these slots contained internal Ta spring clips welded to tungsten rods (1.0 mm diameter) for ohmic heating of the crystal and for thermal contact. The third slot contained a chromel-constantan thermocouple (type E, 0.076 mm diameter) which is spot welded into the center of a Ta spring clip which is inserted into this upper slot [22]. To further assure intimate crystal-thermocouple contact, a tungsten pressure clip spans the area behind the crystal and is spring loaded between the upper and lower

slots. This method has been found to be entirely satisfactory for programmed heating and cooling of the crystal in the temperature range 100 - 1200 K. A modified digital temperature programmer [26] was used to reproducibly heat the crystal at a linear rate over most of the temperature range. A variety of heating rates are possible. A picture of the general mounting procedure, and a complete description of the crystal mounting method may be found in reference [22].

The crystal was chemically cleaned using a methanol rinse prior to insertion in the ultrahigh vacuum system. Glancing incidence Ar^+ ion bombardment, followed by heating in vacuum at 1190 K for ~ 5 min, then cooling (rate ~ 1 K/S), was found to produce a clean Si(100) crystal giving a reproducible (2 x 1) LEED pattern. The fact that the (2 x 1) pattern did not contain significant (1 x 2) LEED intensity indicates that there is a preferential distribution of (2 x 1) domains having a single orientation on this crystal.

We estimate, on the basis of the signal-to-noise ratio in the Auger spectrum for the cleaned Si crystal, that the limit of detectability for the following impurities in the Auger sampling depth are: C (272 eV) = 3.3%; N (381 eV) = 1.4%; O (511 eV) = 0.9%; Ni (848 eV) = 2.6%. However, none of these common impurities in Si were actually detected by Auger spectroscopy on our clean crystal.

III. EXPERIMENTAL RESULTS

A. NH_3 Adsorption Experiments at 120 K

Figure 4 illustrates a typical experimental measurement of the adsorption kinetics for NH_3 adsorption by Si(100) at 120 K, using the

directed beam doser technique. The figure shows the mass spectrometer response to various operations in the apparatus. With the crystal out of the beam, NH_3 is admitted to the doser at a time of 100 seconds, and in the interval 100 - 160 seconds, little response is observed with the mass spectrometer. This behavior is due to adsorption of NH_3 on the walls of the 10 μm diameter walls of the microcapillary array (a phenomenon which has been observed previously [7]). Beyond 160 seconds, NH_3 begins to exit from the capillary array doser and the mass spectrometer signal rises monotonically as the inner surfaces of the microcapillary array saturate with adsorbed NH_3, and as the regions of the UHV system exposed to NH_3 also saturate. Thus, the fluence of NH_3 into the UHV system is becoming larger as time increases due to the saturation of the capillary array. Near 600 seconds, we assume that the doser is saturated. In fact, a calculation based on the fluence of NH_3 entering the capillary array (~ 50 cm^2 internal surface area) indicates that about 1 monolayer of NH_3 would have been intercepted by the inner surface of the array in 500 seconds of operation with 1.040 Torr NH_3 backing pressure behind the 2 μm conductance-limiting orifice in the doser apparatus. Auger measurements of the clean Si surface which was located out of the NH_3 beam, indicate that surface contaminants are below detectible limits during this initial period of random flux exposure.

At 600 seconds, the clean Si(100) crystal is rotated into the NH_3 beam, and a rapid decrease in NH_3 signal received by the QMS is observed. The horizontal plateau observed in the time interval 610 - ~ 660 seconds corresponds to an adsorption process on the crystal which proceeds with unity sticking probability, S = 1, to within the accuracy of our measurement methods. The fact that this section of the uptake

curve is accurately horizontal is evidence that the microcapillary array has become saturated by 500 seconds of operation. The ratio $\Delta_1/(\Delta_1 + \Delta_2)$ therefore corresponds to the fraction of NH_3 which is intercepted by the crystal. The average intercepted fraction is measured to be 0.33 ± .04 for our doser-crystal geometry. The value 0.33 is in fair agreement with calculations based on the geometry of the doser and the crystal where the calculated fraction intercepted is ~ 0.6 [24]. The NH_3 exposure to the crystal at the end of the plateau corresponds to $3.4 \pm 1.0 \times 10^{14}$ NH_3/cm^2. [Note: the error in this measurement is not an average deviation but is the result of a total propagation of error treatment of the experiment]. At 660 seconds, the rapid adsorption process on the crystal is complete, and a slower adsorption process with constantly decreasing rate of adsorption takes place, causing the reflected NH_3 flux from the crystal to rise as shown. When the crystal is rotated out of the NH_3 beam at 925 s, the reflected NH_3 signal received by the mass spectrometer falls to a value corresponding to randomization in the vacuum system of the limiting fluence of NH_3 into a vacuum system whose walls are nearly saturated with NH_3. Upon turning the NH_3 beam doser off, the delivery of some NH_3 to the vacuum system continues as desorption of NH_3 occurs from the inner walls of the microcapillary array, and from the vacuum system walls. This causes the mass spectrometer signal to slowly return to its starting value.

B. Temperature Programmed Desorption from NH_3/Si(100)

Figure 5 shows a series of temperature programmed desorption (TPD) spectra for NH_3 adsorbed at 120 K on Si(100). The heating rate, $\beta = dT/dt$, for these measurements is $\beta = 1.6$ K/S. At low exposures to NH_3, little

NH_3 desorption is observed from the crystal. As the exposure increases a high temperature NH_3 desorption feature is observed with its peak temperature (T_p) near 650 K. This feature intensifies and shifts to T_p = 670 K at the highest exposures shown. This 650 K-desorption process is due to the recombination of adsorbed NH_2 species with H(a) species to liberate NH_3, as will be shown later. In addition to the high temperature NH_3 desorption process, we also observe a sequence of low temperature NH_3 desorption states forming below 350 K as the NH_3 exposure is increased (not shown in full). These low temperature states are due to weak chemisorption and multilayer condensation of undissociated NH_3 onto the surface as the exposure to NH_3 is increased and will not be discussed here. Assuming that the desorption process is first order for the high-temperature NH_3 species, we have used the method of Redhead [27] to estimate the first order kinetic parameters associated with this desorption process, finding that E_d = 46 kcal./mole, and assuming ν_1 = 10^{14} s^{-1} for NH_3 coverages near 3.4 x $10^{14}/cm^2$.

Figure 6 shows the H_2 temperature programmed desorption which follows the liberation of NH_3 shown in Figure 5. It is seen that a single (monohydride desorption) H_2 desorption feature is observed above about 680 K. This H_2 desorption process is initiated following the desorption of the majority of the high temperature NH_3 state. The coverage development of the high-temperature NH_3 and H_2 desorption processes is shown in Figure 7, where the integrated yield in each desorption process is shown as a function of the NH_3 exposure at 120 K.

It should be noted that at the end of the plateau in Figure 4, the adsorption uptake (3.4 ± 1.0 x 10^{14} NH_3/cm^2) of strongly chemisorbed species derived from NH_3 is of the order of 85% complete, judging from the

H_2 desorption behavior (Figure 7) which increases by 14% above this exposure. Thus, the H_2 desorption data, coupled with the uptake data (Figure 4), would indicate that the saturation coverage of NH_2-producing NH_3 species on Si(100) is $3.9 \pm 1.2 \times 10^{14}$ NH_3/cm^2. We interpret this to indicate that one $NH_2(a)$ species may form per Si-Si dimer site, since the perfect Si(100)(2x1) crystal would present 3.4×10^{14} Si-Si dimer sites/cm^2.

Figure 8 shows a comparison between the TPD spectra for the products of NH_3 adsorption compared to the desorption of H_2 from Si(100) covered with adsorbed hydrogen (produced by bombardment from a hot W-filament atomic H source). The heating rate for these measurements is $\beta = 0.9$ K/S. The hydrogen desorption from NH_3 decomposition closely resembles that from monohydride H(a) desorption from H/Si(100) (a slightly lower maximum peak temperature is noted for the H_2 from NH_3). This indicates that the desorption of H_2 is controlled by hydrogen desorption-limiting surface kinetics when it is produced from NH_3. On the other hand, the NH_3 desorption in the high temperature NH_3 state below the H_2 desorption temperature occurs under conditions where all H(a) from NH_3 decomposition is present to act as a source of H(a) for recombination with $NH_2(a)$ species.

C. Deuterium-Ammonia Coadsorption Studies

In order to demonstrate that NH_3 liberation in the high-temperature desorption state is due to a recombination process of H(a) with $NH_2(a)$ species, atomic D(a) was preadsorbed, followed by NH_3 adsorption at 120 K.

It has been shown that deuterium (or hydrogen) on Si(100) forms a

monohydride phase (one D for every Si dangling bond) followed by a dihydride phase (two D on every other Si atom for a saturation coverage of 1.5 D/Si). At hydrogen coverages above the monohydride stage, Si surface reconstruction occurs in which the Si-Si dimer bonds are broken after saturation of the monohydride phase on Si(100) [28,29].

The thermal desorption of $D_2(g)$ from Si(100) as a function of the coverage of D(a) exhibits two desorption features: the monohydride at ~ 780 K and a dihydride feature at ~ 675 K [30]. The monohydride feature is seen for all atomic deuterium exposures. The dihydride desorption feature is observed only above D(a) monolayer coverage [29]. From the thermal desorption spectra obtained in our system, it is possible on the basis of the sequential development of monohydride and dihydride desorption states, to accurately calibrate the coverage of D(a). It should be noted that exposures of atomic D are expressed as Langmuirs [1L = 1 x 10^{-6}Torr-sec] of D_2 exposed to the hot W-spiral described previously. It is found, under our experimental conditions, that the dihydride phase is first detected at 6L D_2 as shown in Figure 9. This means that 6L exposure (to D from D_2) will place 1 D/Si on the Si(100) surface as a monohydride species (6.8 x 10^{14} D/cm^2).

The preadsorption of deuterium on Si(100) caps the active adsoption sites for NH_3. This is clearly demonstrated in Figure 10 where the adsorption kinetics for NH_3 are shown for various levels of coverage of preadsorbed D. The effect of the preadsorbed D on the adsorption of NH_3 is to shorten the constant sticking coefficient (S=1) region and to diminish the rate of NH_3 adsorption beyond the end of the plateau. The effect on the slow NH_3 adsorption process is observed by the increasing slope of the curves in this region as the coverage of D(a) is

increased. It should be noted that at a coverage of 7.9×10^{14} D/cm^2 (= 1.16 D/Si) no ammonia adsorption occurs, indicating that to within our experimental error a saturated monohydride layer of D(a) (= 1 D/Si) effectively passivates the Si(100) surface for ammonia adsorption. Such passivation by preadsorbed H has also been seen for olefin adsorption on the Si(100) surface [25].

For D(a) coverages corresponding to less than ~ 1 D/Si, it is possible to adsorb NH_3, producing NH_2(a) species as will be shown. Subsequent heating of the coadsorbed D(a) and NH_2(a) on Si(100) produces the following desorption species: H_2, HD, D_2, NH_3, NH_2D, NHD_2, and ND_3. The isotopic ammonia desorption species are shown in the insert to Figure 11 for a single experiment.

If ammonia were to molecularly adsorb and then desorb, little or no isotopic mixing would probably occur. Such behavior was observed on the surface containing D(a) for NH_3 thermal desorption below 350 K, where NH_2D, NHD_2 and ND_3 were not seen (not shown). Thus the weakly bound NH_3 does not undergo isotopic exchange with D(a) prior to its desorption as NH_3.

The formula of the NH_x(a) species which recombine with H(D)(a) near 700 K may be determined from the ratios of the desorbing NH_xD_{3-x} species (x = 0, 1, 2, 3). In Figure 11, the relative yields of the NH_xD_{3-x} species are shown as a function of D(a) precoverage of the Si(100) surface. Since NH_2D predominates as a desorption product compared to NHD_2 and ND_3 species over the entire D(a) coverage range, it follows that NH_2(a) is the majority surface species resulting from the dissociative adsorption of ammonia on Si(100). The NHD_2 and ND_3 species arise from consecutive isotopic exchange processes through the surface reactions:

$$NH_2(a) + D(a) \rightarrow NHD(a) + H(a) \xrightarrow{D(a)} NHD_2(g) \quad (1)$$

$$NHD(a) + D(a) \rightarrow ND_2(a) + H(a) \xrightarrow{D(a)} ND_3(g) \quad (2)$$

These results in Figure 11 clearly indicate that NH(a), if present at all from NH_3 adsorption, is a minority surface species upon dissociative NH_3 adsorption on Si(100).

A close examination of the NH_3, NH_2D, ND_2H and ND_3 desorption spectra shown in the inset to Figure 11 shows that the desorption temperature for the deuterated-ammonia species increases progressively for increasing incorporation of deuterium in the isotopic ammonia molecules. This indicates that a deuterium kinetic isotope effect is present. The rate determining step for ammonia desorption is related to the zero point vibrational energy of a hydrogenic species in the elementary step for NH_3 formation from $NH_2(a) + H(a)$. It is likely that this deuterium kinetic isotope effect is due to the loss of an Si-H vibrational motion in the formation of the transition complex for NH_3 production by the recombination step, i.e., speaking approximately, an Si-H vibration is converted to the reaction coordinate for the recombinative NH_3 production step.

D. Auger Spectroscopy Studies of Nitrogen on Si(100) During Heating of an NH_3 Layer

The thermal decomposition of the nitride species on the surface, as monitored by the N(KLL)/Si(LVV) Auger peak-to-peak (p-p) ratio, is shown in Figure 12. An exposure of 8.9×10^{15} NH_3/cm^2 was used in the experiment, and the corresponding TPD spectrum is shown as a dashed curve in

the bottom of the figure. To perform the Auger spectroscopy study, the crystal was exposed to NH_3 and then heated with an identical heating ramp (rate: = 1.6 K/s) to a series of predetermined temperatures. The crystal was then cooled to 120 K and an Auger spectrum was taken at four points on the surface; care was taken to avoid cumulative electron beam effects in the acquisition of the AES data by using different crystal positions throughout the analysis.

The N/Si Auger ratio remains constant in the temperature range from 125 - 625 K and thus does not reflect the decrease in NH_3 coverage below 375 K due to the desorption of molecularly adsorbed NH_3. We believe that the Auger electron beam desorbs molecular NH_3 quickly from the multilayer and therefore measures N Auger intensity only from the strongly-bound NH_2(a) surface species. Since the thermal chemistry of the strongly-bound NH_2(a) state is responsible for nitride formation, we focus our study on this state.

The N/Si Auger ratio remains almost constant at 0.18 in the 600 - 700 K temperature range. The TPD spectrum, however, indicates that recombination of the NH_2(a) species with H(a) produces the observed NH_3(g) desorption process seen at 660 K. Apparently, the recombinative desorption channel available to the NH_2 adsorbate is a minor one, and most of the NH_2(a) species remain on the surface to undergo further decomposition to form a nitride layer, liberating H_2 above ~ 680 K.

Increasing the crystal temperature beyond 725 K confirms that nitride formation is occurring as a decrease in N/Si Auger ratio is observed. Since a desorption pathway of NH_3 or N_2 is not observed above 725 K, we conclude that N(a) diffusion into the bulk is responsible for the decrease in N(KLL) intensity seen above 725 K. Indeed, this obser-

vation is consistent with thermal nitridation studies of the Si surface reported previously [3,10,12,13,31], where nitride formation from NH_3 occurs above about 700 K.

An assay of the nitrogen coverage produced upon NH_3 adsorption and its behavior upon heating to 1000 K is shown in Figure 13. An increase in the N/Si Auger ratio is observed until an exposure of ~ 6×10^{14} NH_3/cm^2 is attained, where saturation of the N Auger signal is evident. This saturation exposure is in excellent agreement with the adsorption data presented in Figure 4, where the horizontal plateau (corresponding to a unity sticking probability) corresponds to an exposure of $3.4 \quad 1.0 \times 10^{14}$ NH_3/cm^2 at which point NH_3 adsorption is 86% complete (see Figures 4 and 7 and discussion thereof). Assuming that there are 3.4×10^{14} Si-dimers/cm^2 at the Si(100) surface (corresponding to 6.8×10^{14} Si atoms/cm^2) we conclude on the basis of the uptake measurements (Figure 4), the TPD measurements of H_2 desorption (Figure 7), and the N Auger measurements (Figure 13) that there is 1 NH_2 plus 1 H per Si-Si dimer on the Si(100) surface upon saturation.

We also note that upon thermal activation to 1000 K, the reduction in N/Si Auger ratio to ~ 60% of the initial value is consistent with the formation of a nitride layer, and with penetration of surface N atoms into the near surface region [5], as may be seen in Figure 13, and by comparison with Figure 12.

E. LEED Studies of Si(100)

Figure 14 shows the LEED patterns obtained from the Si(100) crystal when it has been studied in two azimuthal orientations in the apparatus, obtained by removing the crystal from its holder and rotating

it by 90°. In Figure 14a, a single (2 x 1) unit cell is clearly observed indicating that the predominant orientation of the reconstructed surface is as shown in the upper panel in which the Si-Si dimer structures are orientated with their Si-Si axes almost in the vertical direction. Upon rotation of the crystal by 90°, as shown in Figure 14b, the (2 x 1) unit cell is observed to rotate as shown, and evidence for some contribution from the superposition of an unrotated (1x2) structure is also observed. Since the separate LEED measurements cannot be made at exactly the same location on the crystal, we cannot statistically determine, for the entire crystal, the fractional orientation of domains in each direction, but based on the symmetry of the ESDIAD patterns to be shown later, we believe that the crystal exhibits a preferential statistical orientation of Si(100)-(2 x 1) domains as is observed by LEED in Figure 14a. Such effects have been observed by others for Si(100) [32].

F. ESDIAD Studies of Adsorbed Species Produced from NH_3 on Si(100)

H^+ ESDIAD patterns are clearly observed from the Si(100) crystal containing NH_3-derived surface species, in agreement with previous work [19]. In our apparatus there is observed a systematic attenuation of these ion patterns by the shadow of the drift tube of the electron gun, an effect seen previously [33]. A symmetrization-smoothing procedure has therefore been developed which disregards the information coming from the electron gun side of the pattern in an unbiased manner. Figure 15 illustrates this, and also shows the effect on the H^+ ESDIAD pattern of

rotating the crystal azimuthally as was done for the LEED measurement in Figure 14. Figure 15a shows the H^+ ESDIAD pattern obtained with the crystal oriented as in Figure 14a (before crystal rotation). A broad base of H^+ ion emission is observed in the ESDIAD pattern shown to the left, and on top of this base projects a fin shaped feature which can best be seen in the contour diagram shown below the three dimensional figure. The contour diagram clearly shows the attenuation due to the drift tube shadow on the left hand side. This contour diagram involves contour levels which emphasize the ESDIAD fan-shaped structure above the broad base of H^+ emission. To eliminate the effect of the electron gun drift tube in the pattern, a mirror plane is established through the maximum point of the ESDIAD pattern, and all data to the left of the mirror plane are disregarded. The right hand side of the pattern is then reflected across the mirror plane as shown in the middle panels. Finally, we employ a symmetrization-smoothing technique in which an averaging of all points 180° apart around the center of the pattern is employed, as has been reported previously [34]. It can be seen in the top of Figure 15 that the overall two-fold symmetry of the H^+ ESDIAD data, seen in the unprocessed data on the left, is refined and smoothed by the two image enhancement procedures, but the basic pattern symmetry is not in any way introduced by our processing of the data. An elliptical shaped contour pattern of H^+ emission, superimposed on a broad featureless plateau of H^+ emission is observed. The long axis of the ellipse is accurately perpendicular to the $\langle 01\bar{1} \rangle$ direction, i.e. perpendicular to the predominant Si-Si bond direction on the crystal.

A critical test of these observations was obtained after the azi-

muthal rotation of the crystal as shown in Figure 15b. Here the raw data show that the elliptical H^+ emission has rotated by 90°. Use of the mirror plane and two-fold symmetrization procedures refines the patterns. The rotation of the major axis of the H^+ ESDIAD pattern, compared to the upper figures, again suggests that an elliptical pattern is being observed which is correlated with the preferential orientation of the Si-Si dimer bonds, and that the long axis of the H^+ ellipse (indicated by arrows) is accurately perpendicular to these Si-Si dimer bond directions.

The ESDIAD measurements shown in Figures 15a and 15b were obtained at partial coverage of NH_3 on Si(100), where none of the low temperature NH_3 states are observed by temperature programmed desorption. It was therefore of interest to compare ESDIAD results as a function of coverage, and this is shown in Figure 16. Beginning at the bottom of the figure we see that at an NH_3 exposure of 1.1×10^{14} NH_3/cm^2 (0.3 monolayers of NH_2), the elliptical H^+ ESDIAD pattern is still obtained, but that the ellipticity is not so pronounced. The ESDIAD pattern previously shown in Figure 15 is shown in the middle of Figure 16 for an NH_2 coverage of 0.6 monolayers. Finally, for a higher exposure to NH_3 (11.1×10^{14} NH_3/cm^2), a third H^+ ESDIAD pattern which shows little evidence for ellipticity is observed. At this high NH_3 exposure, the undissociated NH_3 molecules which desorb at low temperatures are present on the surface, probably as a second layer above the NH_2(a) plus H(a) surface species produced by dissociative adsorption at 120 K.

Since we postulate that NH_3 dissociates at 120 K to produce NH_2(a) plus H(a), it was of interest to determine whether ESDIAD could detect changes due to thermal effects from the adsorption temperature (130 K)

up to the $NH_2(a) + H(a)$ recombination temperature (~ 600 K). Experiments with this objective are shown in Figure 17, where 4.9×10^{14} NH_3 molecules/cm^2 were adsorbed at 130 K at the beginning of the experiment. The elliptical H^+ pattern is observed to slowly attenuate while retaining its ellipticity up to 642 K, where recombination has begun to occur. Thus we may say on the basis of these ESDIAD observations that a fraction of the $NH_2(a)$ species produced at 130 K retain their structural character up to the point where recombination and subsequent desorption or complete dissociation take place. This conclusion is confirmed by studies of the H^+ ion yield versus temperature as shown in Figure 18. Here it is observed for NH_3 coverages where the second-layer NH_3 species have not yet formed to anv great extent, that a slow decrease in the H^+ yield occurs from ı20 K up to about 650 K; above 650 K, all remaining H^+ yielding species are destroyed thermally. These results also show that H(a), produced by NH_3 or NH_2 dissociation, does not yield H^+ with a high ESD cross section, since H_2 desorption does not occur until one reaches about 680 K, a temperature where the H^+ ESD yield has vanished in our experiments shown in Figure 18. The very small ESD yield of H^+ from Si(100) was confirmed by separate ESDIAD studies in this laboratory in which pure atomic H was adsorbed on Si(100).

G. Measurements of the H^+ Ion Energy Distribution from $NH_2(a)$ on Si(100)

By use of the ESDIAD hemispherical analyzer in the retarding potential mode, placing a retarding voltage on grid G_3, it was possible to make a measurement of the kinetic energy distribution of H^+ ion emission from $NH_2(a)$ species during ESD. The measurements of the integral ion

collection curve and the derived energy distribution curve (dashed line) are shown in Figure 19. The most probable energy for the H^+ ions is 2.2 eV, in a broad energy distribution with FWHM = 4.1 eV. ESDIAD patterns were acquired at different retarding voltages to determine whether the elliptical (or fin shaped) pattern could be separated from the broad plateau of H^+ emission on which it sits. Figure 20 shows three results of this experiment where a cross section through the ESDIAD pattern along the long axis of the elliptical pattern is displayed. The ratio of the height of the plateau to the total height of the pattern remains in the range 35-40% for all three patterns, suggesting that the H^+ ions in the plateau-base region cannot be separated on the basis of their kinetic energy from the H^+ ions in the upward-projecting ESDIAD fin-shaped pattern which contains the elliptical symmetry when viewed from above.

IV. DISCUSSION OF RESULTS

A. Kinetics of Adsorption of NH_3 on Si(100) at 120 K

The results shown in Figure 4 clearly indicate that NH_3 is initially adsorbed on Si(100) with a constant sticking coefficient at 120 K until an NH_3 exposure of $3.4 \pm 1.0 \times 10^{14}$ NH_3/cm^2 has been achieved. The constancy of the sticking coefficient over this range of coverage is consistent with the magnitude of the sticking coefficient, S, being unity in this range of coverage. Following the initial adsorption, a slower adsorption process occurs, amounting to an additional 14% NH_3 adsorption, as indicated by the hydrogen desorption data in Figure 6 and 7. Hydrogen desorption can thus be used as an index of irreversible NH_3

adsorption.

The behavior of the sticking probability observed in these experiments is consistent with the presence of an extrinsic NH_3 precursor [35] which migrates over filled sites until locating a site where chemisorption can occur. At higher coverages, the average precursor migration distance to a chemisorption site increases, and the surface lifetime of the precursor species begins to limit the ability of the adsorbate molecule to find a chemisorption site before desorption from the precursor occurs. Thus, at higher coverages, the sticking probability falls below unity and the chemisorption process becomes inefficient. The ability to form a second-layer extrinsic precursor is supported by the observation at higher coverages of weakly-held NH_3 molecules which desorb at lower temperatures than the chemisorbed underlayer formed previously. The data measured in our experiments do not permit the detection of a possible intrinsic precursor NH_3 species on Si(100) at 120 K.

B. Dissociative NH_3 Adsorption

It is known that at low exposures of Si(100) to NH_3 at 115-130 K (Figures 15-17), elongated H^+ ESDIAD patterns are observed where the axis of elongation is perpendicular to the dominant Si-Si dimer bond direction. This elongated H^+ pattern is evident at lower exposures of NH_3 in all three figures. As will be shown in a later part of the discussion, this characteristic elongated ESDIAD pattern is indicative of the presence of a chemisorbed NH_2 species, even at 115 K. Thus, the chemisorption of NH_3 should be considered to be dissociative, even at these low temperatures. The continued observation of the elongated H^+ ESDIAD pattern in the temperature range 130 - 642 K is indicative of

the high thermal stability of NH_2 on Si(100).

Since our coverage measurements indicate that one NH_3 species is dissociatively adsorbed per surface Si-Si dimer (see section C below), a simple argument in which an NH_2 species and an H species coexist on a single Si-Si dimer is appealing, as shown schematically in Figure 21.

The identification of the amino species (NH_2) as the primary adsorbate resulting from NH_3 dissociative adsorption on Si(100) is strongly supported by the relative recombinative yields of the deuterated ammonia isotopes, as shown in Figure 11 [36]. Although this experiment, involving preadsorption of atomic D on the Si(100) surface, cannot quantitatively discriminate between the presence of pure $NH_2(a)$, and a mixture of $NH_2(a)$ and smaller quantities of NH(a) and N(a), it is very clear from the experiment that NH_2 is the dominant surface species, since the desorption of $NH_2D(g)$ dominates over all other isotopic ammonia species at high D(a) coverages. At low D(a) coverages, NH_3 is the dominant isotopic ammonia species observed from the recombination process, as would be expected.

The recombination process shows a deuterium kinetic isotope effect, with slightly higher ammonia desorption temperatures being observed for increasing deuterium incorporation (see inset, Figure 11). This suggests that Si-H bond cleavage is rate determining in the production of NH_3 in the high temperature recombination process, and that higher D incorporation involving one, two, or three Si-D bond scission steps may be regarded as contributing sequentially to the production of the isotopic ammonia species which desorbs as indicated in steps (1) and (2) shown previously. Thus, the recombinative ammonia desorption is probably governed kinetically by the collision of mobile H adatoms with

$NH_2(a)$, an example of a reaction-controlled surface process rather than a desorption-controlled mechanism. Recent studies in this laboratory have shown that Si-H bond cleavage produces mobile H adatoms via an activation energy barrier of 47 kcal/mole in approximately this temperature range [37]. Assuming a pre-exponential of $\nu = 10^{14}$ s^{-1} and a first order desorption process, the activation energy for recombination of $NH_2(a)$ and H(a), calculated from the data of Figure 5 by the Redhead method (46 kcal/mole) closely approximates the known Si-H activation energy of 47 kcal/mole [37].

C. Saturation Coverage of NH_2 on Si(100)

Our NH_3 uptake measurements from the collimated beam doser (Figure 4), combined with an estimate of the additional uptake during the slow adsorption process (Figure 6 and 7), has permitted us to determine the saturation coverage of NH_2 on the Si(100) surface. For a perfect Si(100) surface, there are 6.8×10^{14} Si atoms/cm^2, or 3.4×10^{14} Si dimers/cm^2 (the (100) plane density). The NH_3 uptake at saturation coverage is $3.9 \pm 1.2 \times 10^{14}/cm^2$ or 1.1 ± 0.3 NH_3/Si dimer. It should be noted that the error in this measurement was obtained from a full propagation of errors in the measurement, and that our precision in the measurement of the saturation coverage is much better.

This measurement of NH_3 coverage strongly suggests that the stoichiometry of the stable species on Si(100) is NH_2; thus, one NH_3 molecule will deliver to each Si dimer site one NH_2 species and one H species, saturating all dangling bonds. The stoichiometry summarized by this view and in Figure 21 is therefore completely consistent with the detection of $NH_2(a)$ through the exchange experiments with surface

D(a), and with the assignment of the H^+ ESDIAD pattern to the NH_2(a) species adsorbed on dimer Si sites (to be discussed in section D below).

D. Postulated Structure of Amino (NH_2) Species on Si(100)

Figure 21 shows the postulated site and configuration for the bonding of an NH_2 amino ligand to a dangling bond site on Si(100). Using the bond angles present in the free NH_3 molecule plus a crude estimate of the projection angle expected for the Si-N bond in this complex, it is possible to predict qualitatively the H^+ ESDIAD pattern which would be generated from the amino species. It must be remembered that various vibrational modes of the NH_2 species will serve to spread the H^+ pattern along directions which are determined by the highest amplitude thermal motions in the complex. One example of an expected high amplitude vibration will involve torsional rotation of the amino complex about the Si-N bond. In order to visualize the excursions of the N-H bond directions due to this torsional motion about the Si-N bond, Figure 22 has been constructed. Here, the Si-N bond has been directed at an angle of 35 degrees from the normal, which is the observed Si-F bond angle for fluorine adsorption on Si(100) dimer sites [38,19]. The Si-N-H bond angle is taken to be 106.8°, which is the H-N-H bond angle in the NH_3 molecule. Allowing the N-H bond to project in all directions permitted by rotation about the Si-N bond will result in an arc projection, yielding H^+ ions which describe an arc with a maximum lateral excursion from the normal of 38° as shown in Figure 22, where a single N-H bond directed upwards is shown for clarity. The intensity in these arcs is probably attenuated at large polar angles because of reneutralization effects which are favored at high polar

angles. The combination of "right-directed" and "left-directed" NH_2 groups should yield a pair of arc patterns which overlap to form an elliptical pattern as shown in the bottom of Figure 22. For the Si-Si-N bond angle assumed (125°) and the assumed Si-N-H bond angle (106.8°), we estimate that the angular width of the minor axis of the elliptical H^+ ESDIAD pattern will be 76°.

Two additional factors must be recognized in this analysis:

(1) The bond angles used here are only first approximations to the true bond angles. For bonding to Si, it is likely that the Si-N-H bond angle will open to angles above 106.8° due to the larger size of the Si atom compared to a hydrogen atom in NH_3; (2) In addition to the torsional motion discussed above, it is likely that vibrational motions opening the Si-N-H bond will occur (deformation mode) causing a blurring of the H^+ ESDIAD pattern and the resultant filling in of the region between the arcs which will give in this central region a summation of intensity from both the "left-directed" and "right-directed" amino species.

The ESDIAD behavior reported here bears a resemblence to a previous ESDIAD measurement made by Johnson, et al [19], and extends the interpretation made in their work. At low exposures of NH_3 on Si(100) sites, Johnson et al [19] observe a weak halo with H^+ emission predominantly in directions perpendicular to the Si-Si bond directions in the Si dimers. They interpret this to be due to minority adsorbed NH_x species, where "x" is unspecified. Our ESDIAD studies show a fin-shaped H^+ ridge, whose major axis is perpendicular to the Si-Si dimer bond direction. We further identify the species as NH_2 and show that a single NH_2 species per dimer site is produced upon adsorption to full coverage. These results considerably clarify this earlier picture, providing a

stoichiometric, structural, and dynamical view of the adsorbed amino complex. Surface amino complexes have been detected on other surfaces such as Ni(110) [39,40].

E. Origin of the Broad H^+ Angular Distribution

The elliptical H^+ pattern is superimposed upon a broader angular distribution which appears as a base to the elliptical pattern. This broad pattern is not due to molecular NH_3 species adsorbed on top of the NH_2 species, since it is observed at coverages below that required for molecular NH_3 adsorption. At the present time, we believe the most rational explanation is that it is caused by NH_2 species or NH species adsorbed on random defect sites known to be present on Si(100) surfaces from STM measurements [41]. Because of the disorder expected at these sites, a broad azimuthally disordered ESDIAD pattern would be expected. The broad H^+ pattern is present at all coverages, suggesting that the rate of adsorption on the defect sites is similar to the rate on the Si dimer sites (NH_3 sticking probability = unity, initially).

F. ESDIAD Pattern from High NH_3 Coverages

The high coverage- ESDIAD pattern shown in the portion of Figure 16 is almost azimuthally symmetrical, in agreement with the results of Johnson, et al [19], for high NH_3 coverage. We believe this pattern is due to a mixture of H^+ emission from the NH_3 overlayer and an underlayer of NH_2 species. The overlayer-NH_3 species may well be tipped, as observed previously for NH_3 overlayers adsorbed on top of a full layer of CO on Ni(110) [42]. The tipped NH_3 species may be arranged to project an N-H bond in the normal direction, to present little or no azi-

muthal symmetry, and to be uncorrelated with the structure of the underlayer or the Si(100) single crystal.

G. Site Blocking for NH_3 Dissociative Adsorption on Si(100)

Figure 10 presents an informative view of the effect of atomic D adsorbate on Si(100) on the kinetics of adsorption of NH_3. It is observed that both the fast adsorption and the slow adsorption steps are attenuated by blocking by atomic D(H) species. Furthermore, at a surface coverage corresponding closely to a single monolayer of H(a), where each Si dangling bond has been capped to form a Si-H surface species, all dissociative adsorption of NH_3 to form adsorbed NH_2 species is terminated. Similar behavior has been observed for H blockage of olefin interaction with Si(100) surfaces [25,43]. These results suggest that simple bonding ideas involving the utilization of projecting dangling bonds for dissociative chemisorption must be basically true. Indeed, the Si surface provides an ordered array of free radical sites ready to undergo surface chemical reactions which resemble those encountered in free radical chemistry in the gas phase.

The major reaction channel for the dissociation of adsorbed NH_2 involves N-H bond scission at temperatures above about 600-700 K. This process produces adsorbed H(a) which begins to desorb above about 680 K with kinetics that differ only slightly from the desorption of pure H(a) from Si(100). The slightly lower desorption temperature of hydrogen from the NH_2-decomposition route compared to H_2 from pure H(a) may be due to the effect of Si-N bonding in the vicinity of Si-H bonds, possibly reducing the Si-H bond energy slightly. It is likely that promotion of a single Si-H species to a bound, translationally mobile sur-

face hydrogen species [37] occurs when NH_2 is the source of the surface hydrogen, and that the kinetic behavior in the NH_2 + H surface recombination process resembles that measured for pure hydrogen (first order desorption kinetics; E_a = 47 kcal/mole) [37].

A second, minor channel for loss of NH_2(a) involves the recombination with H(a) to produce NH_3(g), which has been discussed in section B above. We believe this recombination channel is a minor channel for decomposition of NH_2(a) based on studies of the N Auger intensities upon heating as shown in Figure 12. Here it may be seen that only a small fractional decrease in the N Auger intensity occurs in the temperature region 600 - 720 K where the recombination process between NH_2(a) and H(a) occurs. Thus, the majority of the NH_3 adsorbed dissociatively as NH_2(a) is effective in delivering atomic N to the surface for formation of a "silicon nitride" layer at elevated temperatures.

H. **Behavior of N(a) on Si(100)**

By about 800 K all hydrogen from NH_2 decomposition has recombined forming H_2(g) which has desorbed. At about 800 K, only atomic N(a) remains on the Si(100) surface. In Figure 12 it may be seen that the N-Auger intensity from the atomic N decreases as N-penetration into the Si(100) lattice occurs. This penetration process continues up to 1000 K, where measurements were discontinued. These results differ in detail from the work of Avouris et al, who report that the N ISS signal from NH_3 adsorption on Si(100) is observed at 90 K, but is not observed at 220 K [3,5]. Their interpretation is that N penetration into Si(100) occurs at 220 K. Our results indicate that NH_2(a) species exist until the dissociation temperature (600 - 700 K), and that N penetration then

occurs beginning at about 700 K. This is consistent with the essentially constant nitrogen Auger intensity seen in Figure 12 up to about 700 K due to the presence of surface NH_2 groups.

V. Summary of Results

The combination of accurate coverage measurements, temperature programmed desorption, Auger spectroscopy, digital LEED, and digital ESDIAD has provided a clear picture of the behavior of NH_3 in its interaction with Si(100).

The following interpretation has been made:

1. Si(100) dimer sites are effective in causing the dissociative adsorption of NH_3 to produce $Si-NH_2$ and Si-H surface species. The saturation coverage of these species is such that the NH_3 dissociatively saturates one Si-Si dimer site. This assignment of NH_2 as the major surface species produced from NH_3 differs from the assignment of Avouris et al, who report that N-H species are produced [6].

2. The NH_2 species is bound to a Si dangling bond site in a structure in which the N-H bonds are projected upwards from the surface; both torsional vibrations around the Si-N bond and low frequency deformations of the $Si-NH_2$ species lead to thermally averaged N-H bond directions which cause a fin-shaped H^+ ESDIAD pattern. The pattern displays its long axis perpendicular to the Si-Si dimer bond direction.

3. The $Si-NH_2$ surface species are stable to about 600 K where some recombine with adsorbed H species to produce $NH_3(g)$ in a minor

reaction channel. The majority of the NH_2 species dissociate to H(a) and N(a) surface species in the temperature range 600-700 K, followed by H_2 liberation. The surface N produced enters into the Si near-surface region at about 700 K. The stability of NH_2 species on Si(100) up to about 600 K followed by dissociation and N-penetration into the bulk above 700 K differs in detail from the interpretation of Avouris et al, who postulate that N penetration occurs near 220 K [3,5].

4. At high NH_3 exposures, molecular NH_3 adsorbs as a second layer and multilayer species. This NH_3 does not participate in dissociative adsorption or in isotopic exchange with Si-D surface species, and desorbs as a molecular species below 300 K. The H^+ ESDIAD patterns obtained at higher NH_3 coverages exhibit a broad, normally-directed geometry indicating that the second layer of NH_3 is probably randomly arranged on the surface.

5. The dissociative adsorption of NH_3 to produce NH_2(a) at 120 K occurs with unity sticking probability until about 85% of the adsorption sites are occupied; above this coverage, the sticking probability of NH_3 decreases as the remainder of the adsorption sites are filled. This behavior is consistent with the operation of a mobile extrinsic precursor adsorption mechanism.

6. Preadsorption of atomic D(H) on Si(100) efficiently blocks NH_3 adsorption and dissociation to NH_2 species. In the limit of

occupancy of all Si dangling bond sites by D(H) adsorbed species, the chemisorption of NH_3 is completely blocked and the surface is passivated. These results are in accordance with the conclusion of Avouris et al [6].

7. H^+ produced by ESD from $Si-NH_2$ species exhibits a most probable ion kinetic energy of 2.2 eV.

8. Evidence is seen for the presence of defect Si adsorption sites which yield H^+ ESDIAD patterns exhibiting a very broad angular distribution from adsorbed species produced from NH_3.

V. Acknowledgement

We gratefully acknowledge the full support of ONR for this work.

References

1. S.M. Sze, Semiconductor Devices, Physics and Technology, Wiley, New York (1985).
2. R.M. Tromp, R.J. Hamers, and J.E. Demuth, Science, 234, 304 (1986); see also R.J. Hamers, R.M. Tromp, and J.E. Demuth, Surface Sci., 181, 346 (1987).
3. Ph. Avouris, F. Bozso, and R.J. Hamers, J. Vac. Sci. Technol., B(5), 1387 (1985).
4. Ph. Avouris, R. Wolkow, F. Bozso, and R.J. Hamers, Materials Research Soc. Symposium Proc., 105 (1988) in press.
5. F. Bozso and Ph. Avouris, Phys. Rev. Lett., 57, 1185 (1986).
6. F. Bozso and Ph. Avouris, Phys. Rev. B38, 3937 (1988).
7. C. Klauber, M.D. Alvey, and J.T. Yates, Jr., Surface Sci., 154, 139 (1985) (see references therein).
8. R.J. Hamers, Ph. Avouris, and F. Bozso, Phys. Rev. Lett., 59, 2071 (1987).
9. R.J. Hamers, Ph. Avouris, and F. Bozso, J. Vac. Sci. Tehcnol, A6, 508 (1988).
10. E.K. Hlil, L. Kubler, J.L. Bischoff and D. Bolmont, Phys. Rev. B35, 5913 (1987).
11. D.G. Kilday, G. Margaritondo, D.J. Frankel, J. Anderson and G.J. Lepeyre, Phys. Rev. B35, 9364 (1987).
12. A. Ermolieff, P. Bernard, S. Marthon and J. Camargo da Costa, J. Appl. Phys., 60, 3162 (1986).
13. J.W. Rogers, D.S. Blair and C.H.F. Peden, in Deposition and Growth; Limits for Microelectronics, A.I.P. Conf. Proc. 167, A.V.S. Series 4, ed. G. Rubloff, 133 (1988).

14. L. Kubler, E.K. Hlil, D. Bolmont and G. Gewinner, Surface Sci., 183, 503 (1987).

15. T. Isu and K. Fujiwara, Solid State Comm., 42, 477 (1982).

16. S. Tanaka, M. Onchi and M. Nishijima, Surface Sci., 191, L756 (1987).

17. M. Nishijima and K. Fujiwara, Solid State Comm., 24, 101 (1977)

18. W.R. Creasy and S. McElvany, Surface Sci., 201 59 (1988).

19. A.L. Johnson, M.M. Walczak and T.E. Madey, Langmuir, 4, 277 (1988).

20. M.J. Dresser, M.D. Alvey and J.T. Yates, Jr., Surface Sci., 169, 91 (1986).

21. M.J. Dresser, M.D. Alvey and J.T. Yates, Jr., J. Vac. Sci. Technol., A4, 1446 (1986).

22. M.J. Bozack, L. Muehlhoff, J.N. Russell, Jr., W.J. Choyke and J.T. Yates, Jr., J. Vac. Sci. Technol., A5, 1 (1987).

23. C.T. Campbell and S.M. Valone, J. Vac. Sci. Technol., A3, 408 (1985).

24. A. Winkler and J.T. Yates, Jr., J. Vac. Sci. Technol., A6, 2929 (1988). Corrections to this calculation were made to account for the angular tilt of the crystal face to the angular distribution of molecules provided by the doser; see D.R. Olander, J. Appl. Phys., 40, 4650 (1969).

25. M.J. Bozack, W.J. Choyke, L. Muehlhoff and J.T. Yates, Jr., Surface Sci., 176, 547 (1986).

26. R.J. Muha, S.M. Gates, P. Basu and J.T. Yates, Jr., Rev. Sci. Instr. 56, 613 (1985).

27. P.A. Redhead, Vacuum, 12, 203 (1962).

28. H. Ibach and J.E. Rowe, Surface Sci., 43, 481 (1974).

29. Y.J. Chabel and K. Ragh Avachari, Phys. Rev. Lett., 54, 1055 (1985); see also Y.J. Chabal, E.E. Chaban and S.B. Christman, J. Electr. Spectrosc. Rel. Phenom., 29, 35 (1983).

30. J. Leifels, Diplomarbeit, Institut fer Festkorperphysik, Univ. Hannover, Hannover (1984).

31. (a) A. Glachant, D. Saidi and J.F. Delord, Surface Sci., 168, 672 (1986); (b) A. Glachant and D. Saidi, J. Vac. Sci. Technol., B3, 985 (1985).

32. For example, S. Sakamoto and H. Hashiguchi, Jpn. J. Appl. Phys., Pt. 2, 25, L78 (1986).

33. M.D. Alvey, M.J. Dresser and J.T. Yates, Jr., Phys. Rev. Lett., 56, 367 (1986).

34. A. Szabo, M. Kiskinova and J.T. Yates, Jr., Surface Sci., 205, 207 (1988).

35. W.H. Weinberg, Kinetics of Interface Reactions, eds. M. Grunze and H.J. Kreuzer, (Springer, NY (1987)), p. 94.

36. P.A. Taylor, R.M. Wallace, M.J. Dresser, W.J. Choyke and J.T. Yates, Jr., Surface Science (submitted).

37. K. Sinniah, M.G. Sherman, L.B. Lewis, W.H. Weinberg, J.T. Yates, Jr. and K.G. Janda, submitted to Phys. Rev. Lett.

38. M.J. Bozack, M.J. Dresser, W.J. Choyke, P.A. Taylor and J.T. Yates, Jr., Surface Sci., 184, L332 (1987).

39. C. Klauber, M.D. Alvey and J.T. Yates, Jr., Surface Sci., 154, 139 (1985).

40. I.C. Bassignana, K. Wagaman, J. Küppers and G. Ertl, Surface Sci., 175, 22 (1986).

41. R.J. Hamers, R.M Tromp and J.E. Demuth, Phys. Rev. B, 34, 5343 (1988).

42. A-M. Lanzillotto, M.J. Dresser, M.D. Alvey and J.T. Yates, Jr., Surface Sci., 191, 15 (1987).

43. M.J. Bozack, W.J. Choyke, L. Muehlhoff and J.T. Yates, Jr., J. Appl. Phys., 60, 3750 (1986).

Figure Captions

Figure 1. Top view of UHV apparatus showing relative positions of instrumentation used.

Figure 2. Cross-sectional, top view of Digital LEED/ESDIAD apparatus.

Figure 3. Calibration of directed beam doser for NH_3 experiments. NH_3 flux entering the chamber is determined by monitoring the backing pressure behind a nominal 2 μm diameter conductance-limiting orifice. The initial two points are not included in the analysis.

Figure 4. Adsorption kinetics for NH_3/Si(100) at 120 K.

Figure 5. TPD spectra from NH_3 on Si(100) at various initial exposures. The NH_3 thermal desorption peak is a result of the recombination of NH_2(a) and H(a).

Figure 6. TPD spectra of H_2 from NH_3 on Si(100) at various initial NH_3 exposures.

Figure 7. Comparison of thermal desorption peak areas (yields) for NH_3 and H_2 as a function of initial NH_3 exposure. The relative yields (uncorrected for QMS sensitivity) indicate that the recombinative desorption channel producing NH_3 is a minor one.

Figure 8. Comparison of TPD kinetics from H/Si(100) and NH_3/Si(100). H_2 desorption is controlled by desorption-limiting surface kinetics when produced from NH_3/Si(100).

Figure 9. Deuterium atom coverage calibration for deuterium-ammonia co-adsorption studies. D_2 exposures are in Langmuirs, uncorrected for gauge sensitivity. Saturation of the mono-

hydride phase has been assumed to be 6.8×10^{14} atoms/cm^2 (dashed line).

Figure 10. Capping of active sites for NH_3 adsorption on Si(100) by D atom adsorption.

Figure 11. Isotopic ammonia desorption yield from deuterium-ammonia coadsorption on Si(100). NH_2D is the principal deuterated ammonia desorption product at all D coverages.

Figure 12. N penetration into bulk as monitored by the N(KLL)/Si(LVV) Auger p-p ratio. The dashed curve represents a TPD spectrum at an NH_3 exposure of 8.9×10^{15} NH_3/cm^2.

Figure 13. Relative assay of nitride species produced by thermal activation of NH_3/Si(100). Adsorption at 120 K reveals saturation of the N Auger signal at an NH_3 exposure of $\sim 6 \times 10^{14}$ NH_3/cm^2.

Figure 14. Digital LEED patterns and their corresponding real-space orientations (a) before crystal rotation, (b) after crystal rotation. The patterns are predominantly (2x1) indicating a preferential statistical orientation of corresponding dimer domains.

Figure 15. Symmetrization procedure used in ESDIAD data from NH_3/Si(100). (a) before crystal rotation. (b) after crystal rotation. In both cases, the ellipticity of the pattern is preserved and the long elliptical axis is oriented perpendicular to the Si-Si dimer bond direction.

Figure 16. H^+ ESDIAD patterns for various NH_3 exposures on Si(100). Orientation of crystal is that in Figure 15(a). The ellipticity of the patterns is pronounced for coverages of

0.3 and 0.6 monolayers of NH_2. At high exposures (11.1 x 10^{14} NH_3/cm^2), a normally directed H^+ beam is observed due to undissociated NH_3 molecules present as a disordered second layer on the NH_2(a) and H(a) species.

Figure 17. Thermal effects on H^+ ESDIAD pattern from NH_3/Si(100). Pattern ellipticity is preserved to 642 K (at the onset of NH_2(a) + H(a) recombination).

Figure 18. H^+ ESD yield as a function of temperature. The H^+ yield is observed from 120 K to ~ 650 K, corresponding to the data in Figure 17. The dashed curve is representative of the NH_3 thermal desorption at high NH_3 exposures. Crystal bias = +100 V.

Figure 19. Measurements of the integral H^+ collection current (solid line) and the derived ion energy distribution (dashed line). The most probable H^+ ion energy is 2.2 eV. Crystal bias = +10 V.

Figure 20. H^+ ESDIAD pattern cross-sections at various retarding voltages. Cross-sections were taken along the major-axis of the corresponding elliptical pattern. These curves suggest that the broad plateau-base of the patterns cannot be separated from the elliptical patterns on the basis of H^+ energy. Curves A, B and C correspond to the data points labeled in Figure 19.

Figure 21. Schematic of the bonding of an NH_2 (amino) ligand and an H ligand to the Si-Si dimer dangling bond sites on Si(100). Dissociative adsorption of NH_3 results in this postulated structure.

Figure 22. Excursions of N-H bond directions due to torsional motion about the Si-N bond. The combination of "left-directed" and "right-directed" species results in the H^+ arc patterns shown in the bottom of the figure. Superposition of the intensities of the arcs combined with N-H dynamical effects due to other NH_2 vibrations results in the elliptical H^+ ESDIAD pattern observed.

Ultrahigh Vacuum Apparatus for Silicon Surface Chemistry

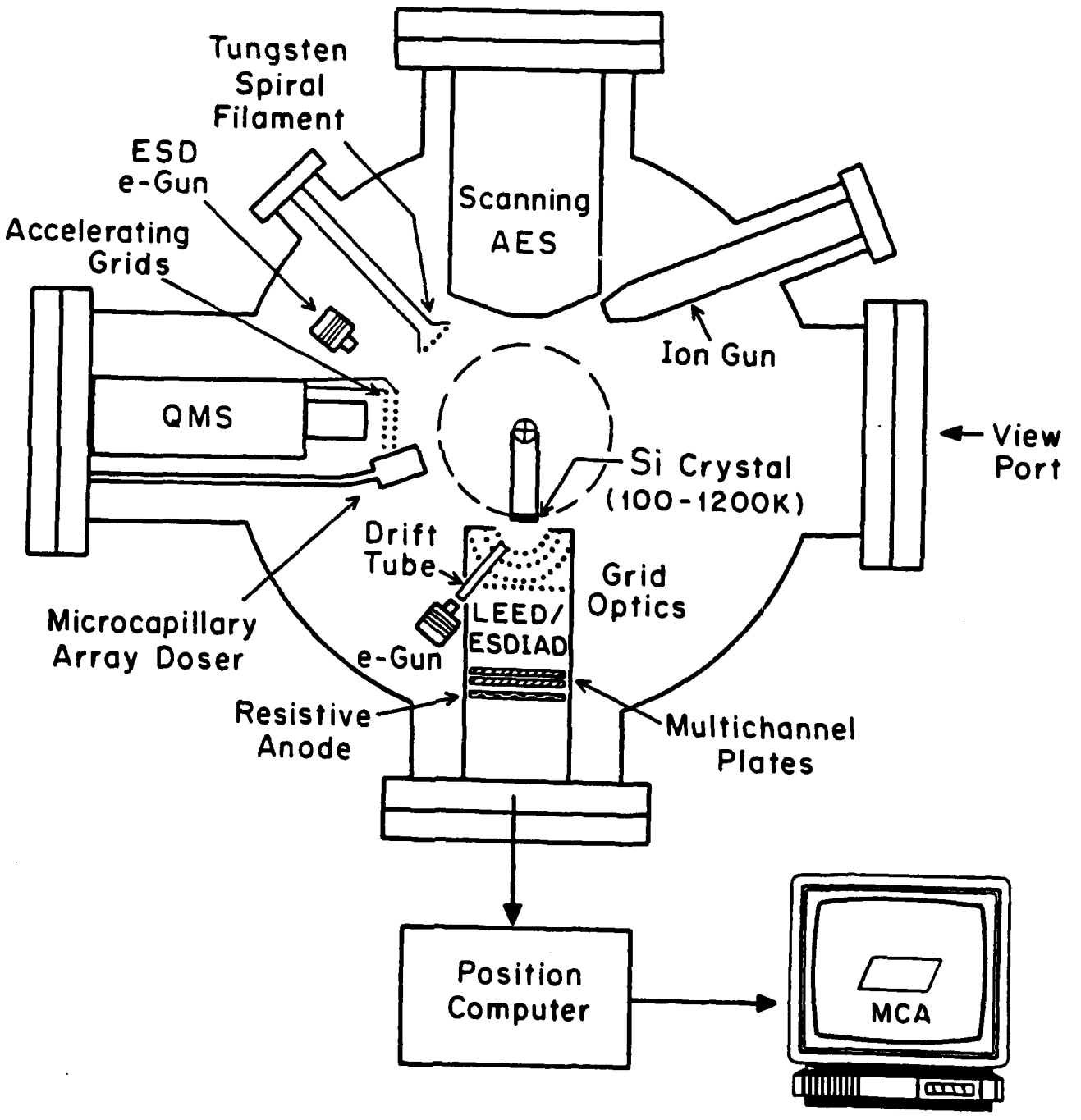

Dresser,
Taylor,
Wallace,
Choyke,
Yates
Figure 1

Cross-sectional View of Digital LEED/ESDIAD Apparatus

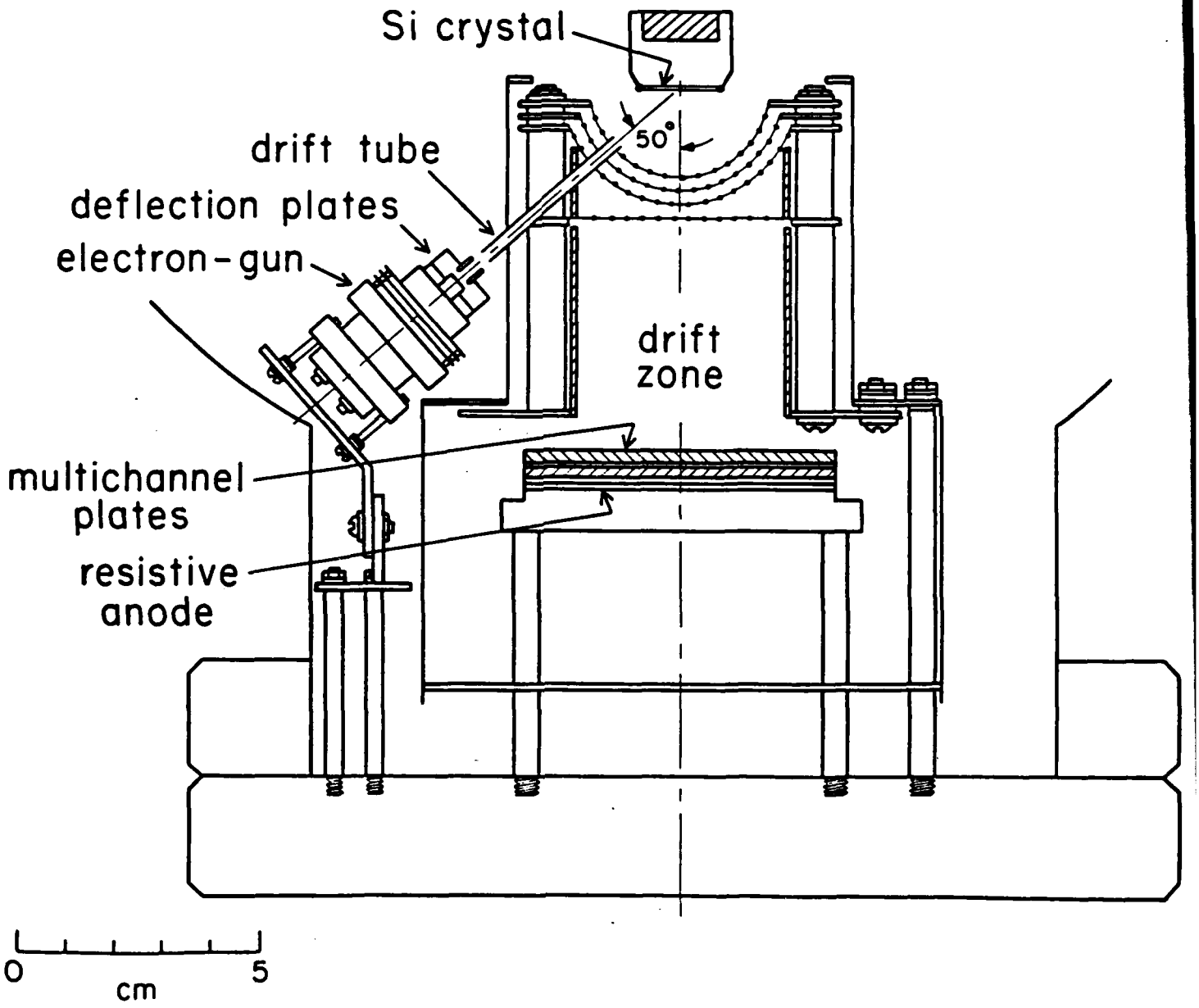

Dresser, Taylor, Wallace Choyke, Yates
Figure 2

Doser Calibration for NH_3

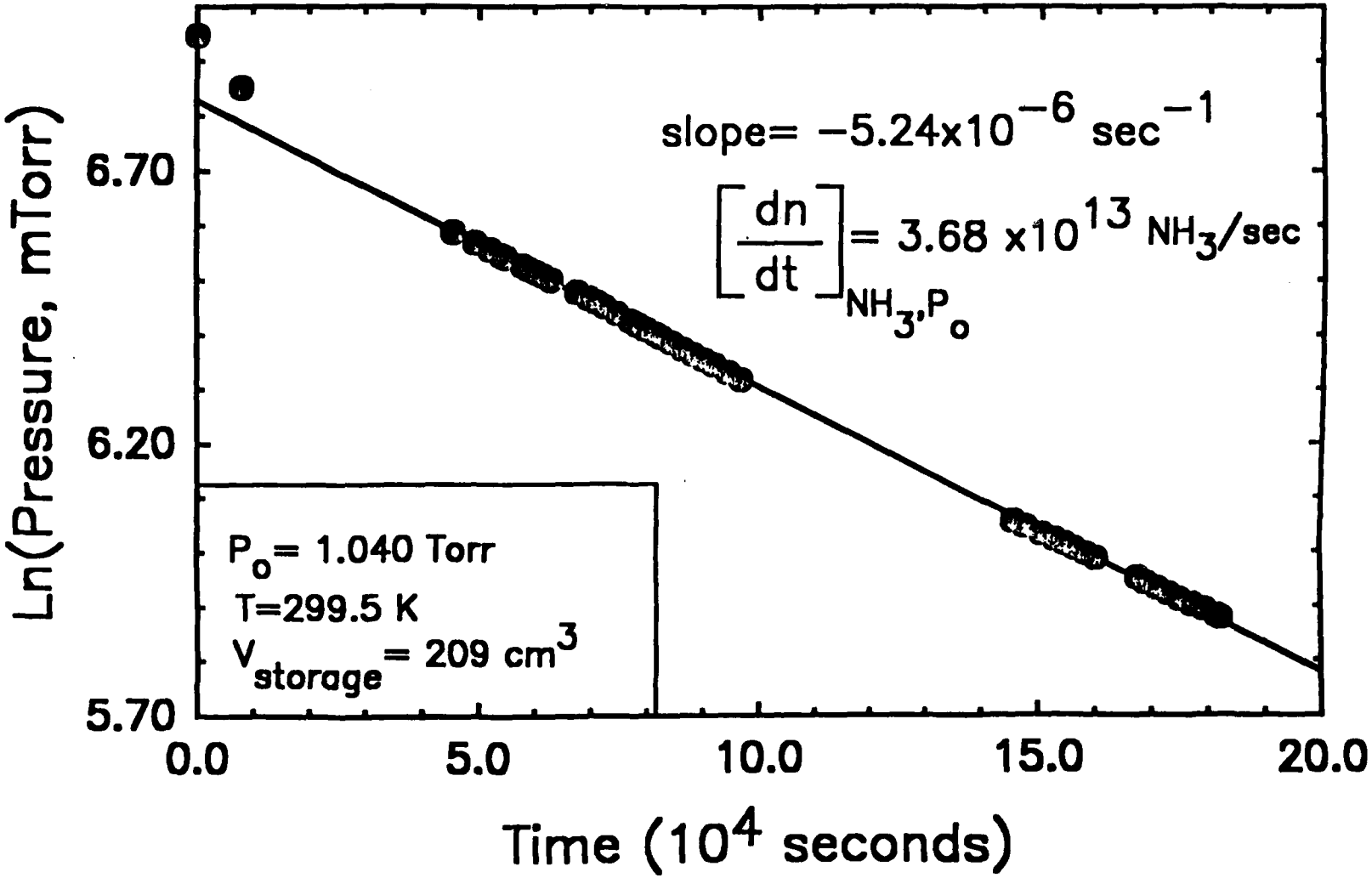

Dresser,
Taylor,
Wallace,
Choyke,
Yates
Figure 3

Adsorption Kinetics : NH_3 on Si(100) at 120K

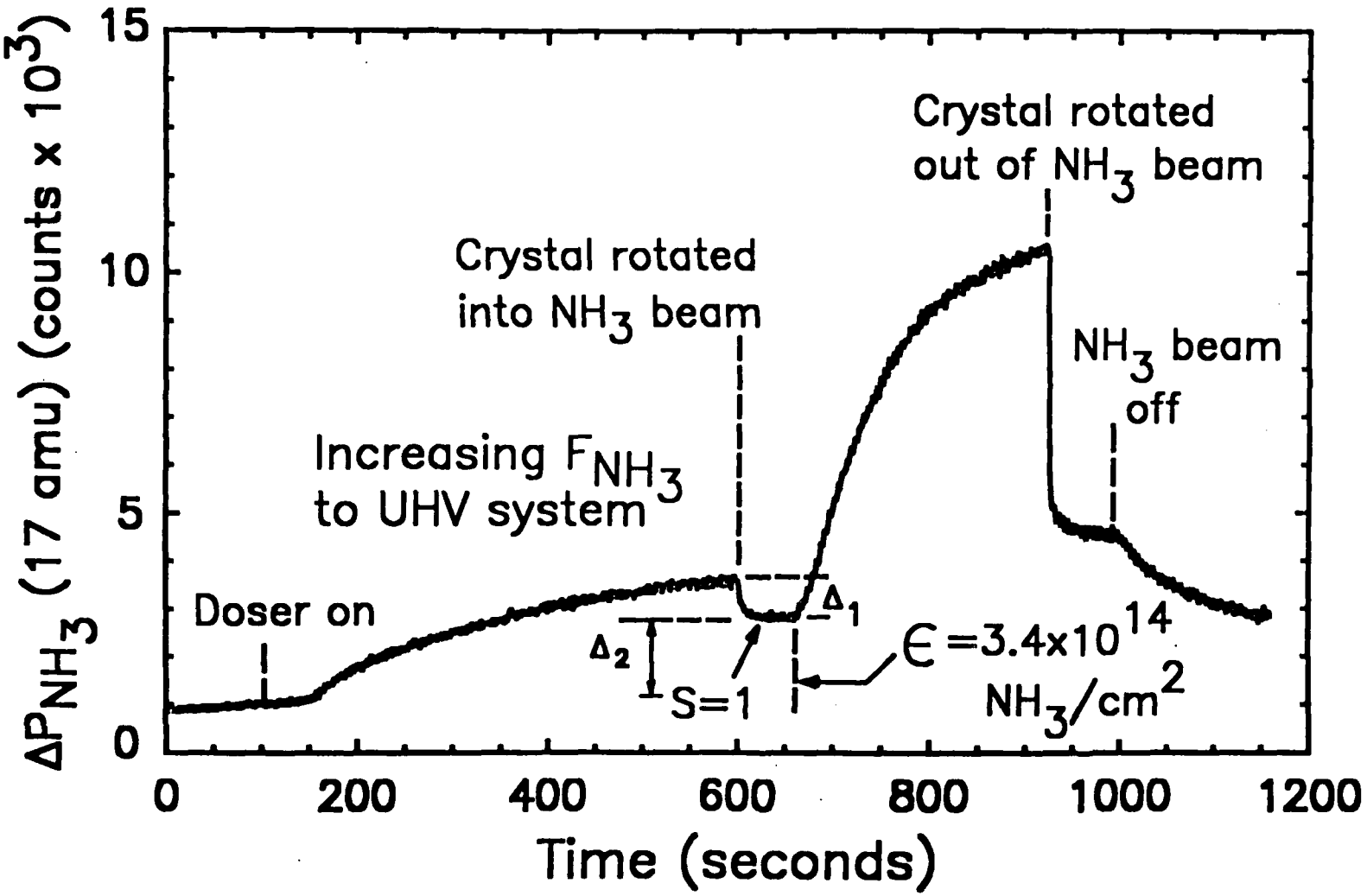

Dresser, Taylor, Wallace, Choyke, Yates
Figure 4

Temperature Programmed Desorptio from Ammonia on Si(100)–(2x1)

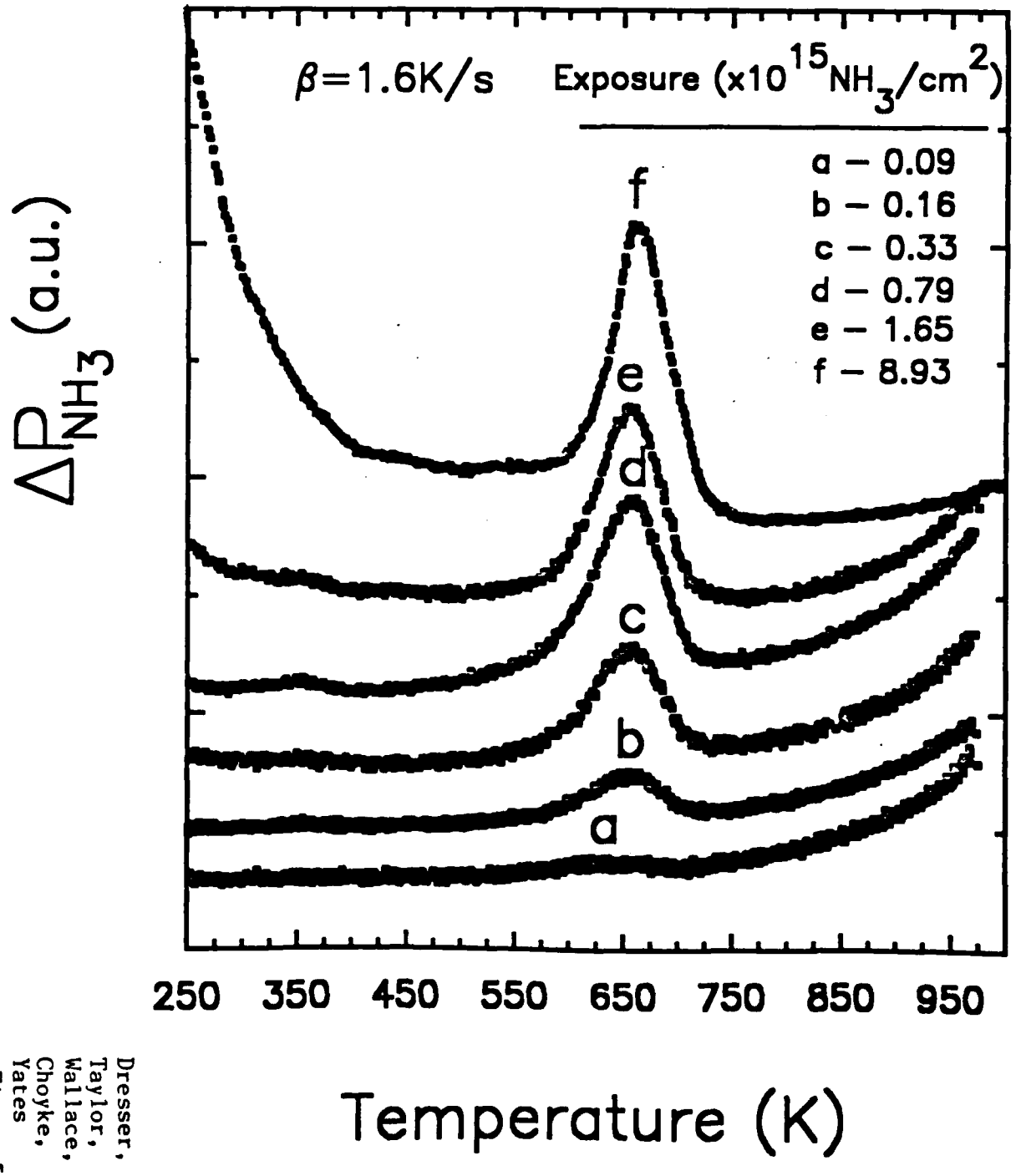

Dresser, Taylor, Wallace, Choyke, Yates
Figure 5

H_2 Temperature Programmed Desorption from NH_3 on Si(100)

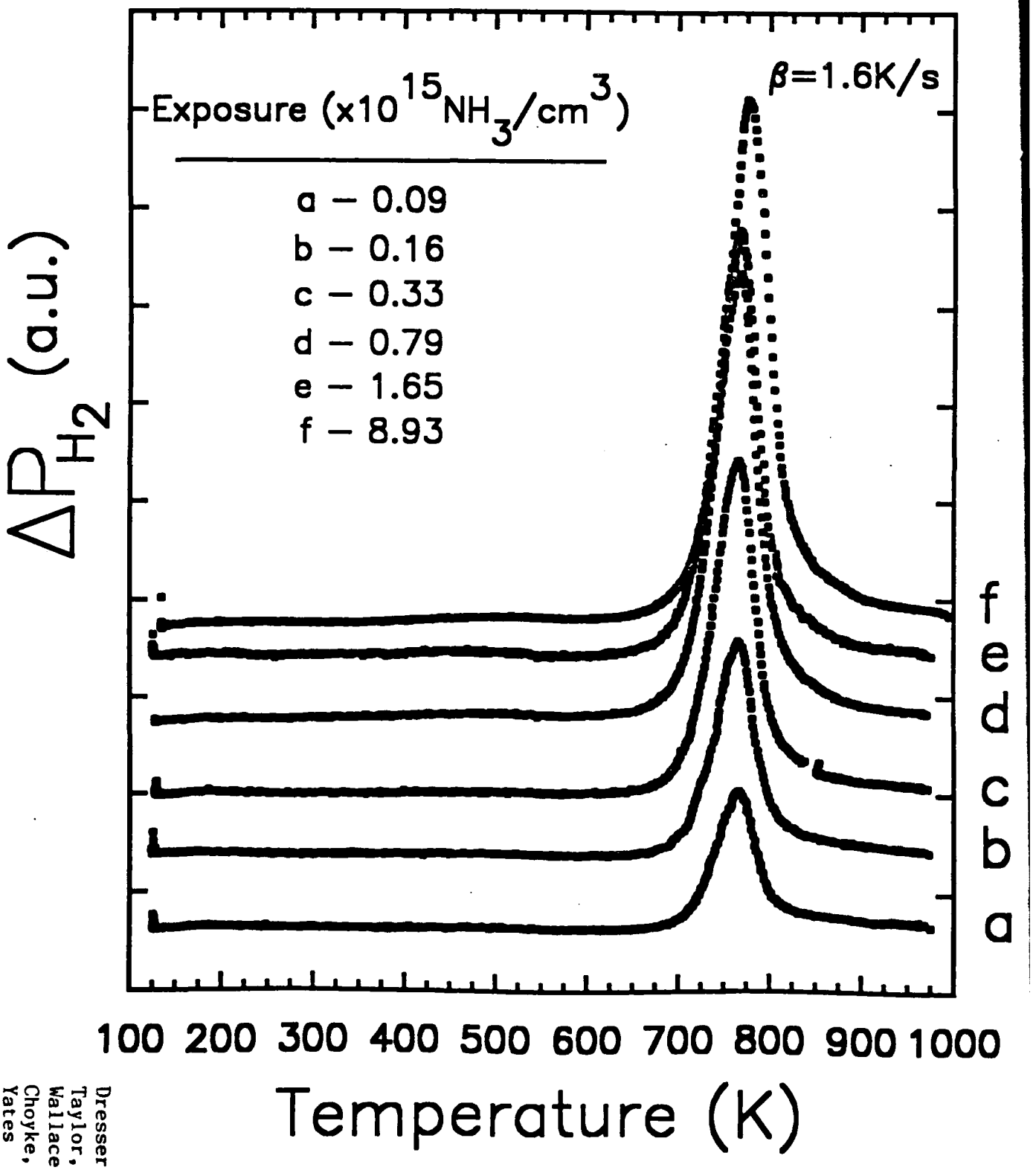

Dresser, Taylor, Wallace, Choyke, Yates
Figure 6

Thermal Desorption Yield from Ammonia on Si(100)

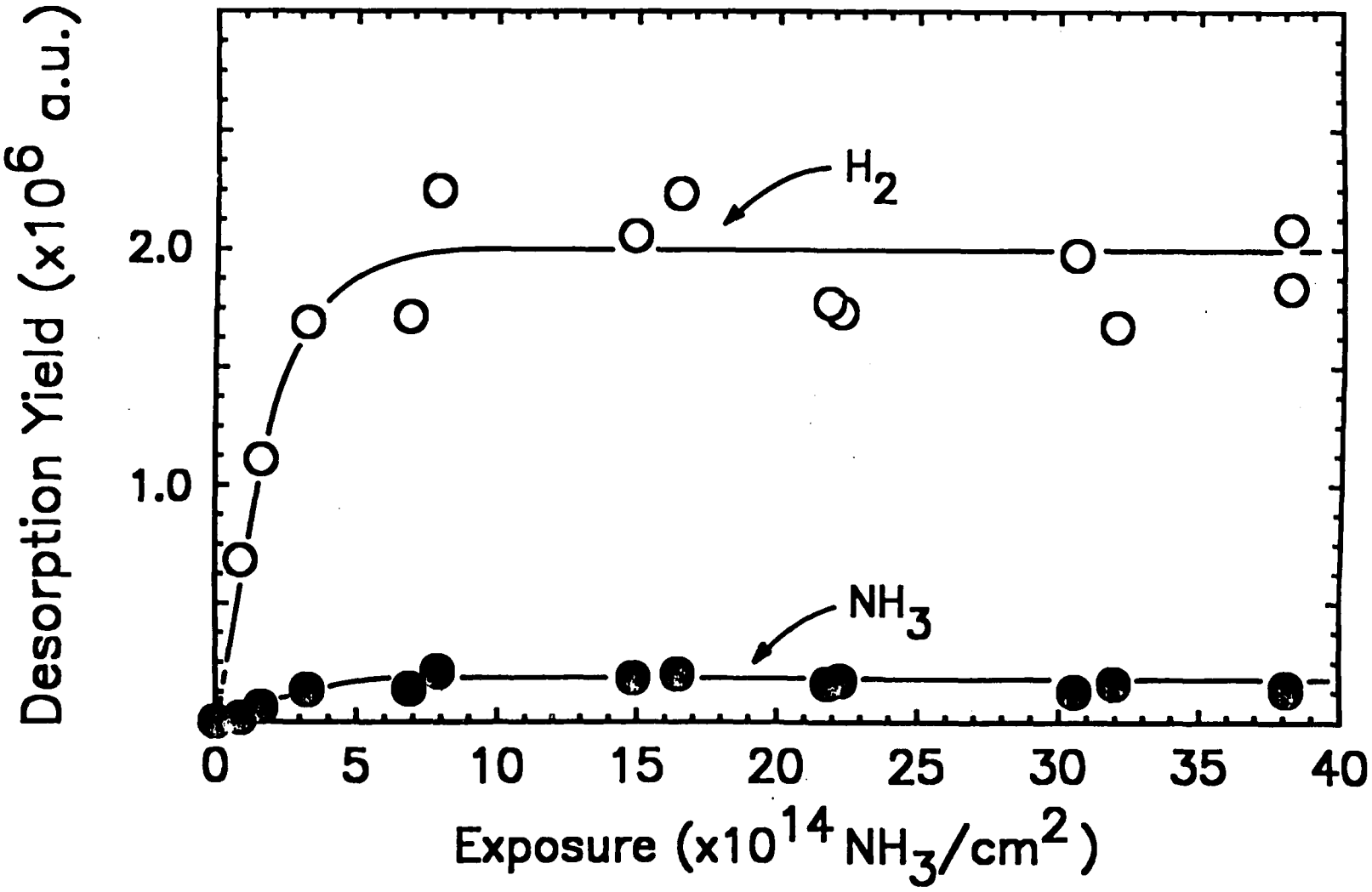

Dresser,
Taylor,
Wallace,
Choyke,
Yates
Figure 7

Comparison of TPD Kinetics for NH_3 and H/Si(100)

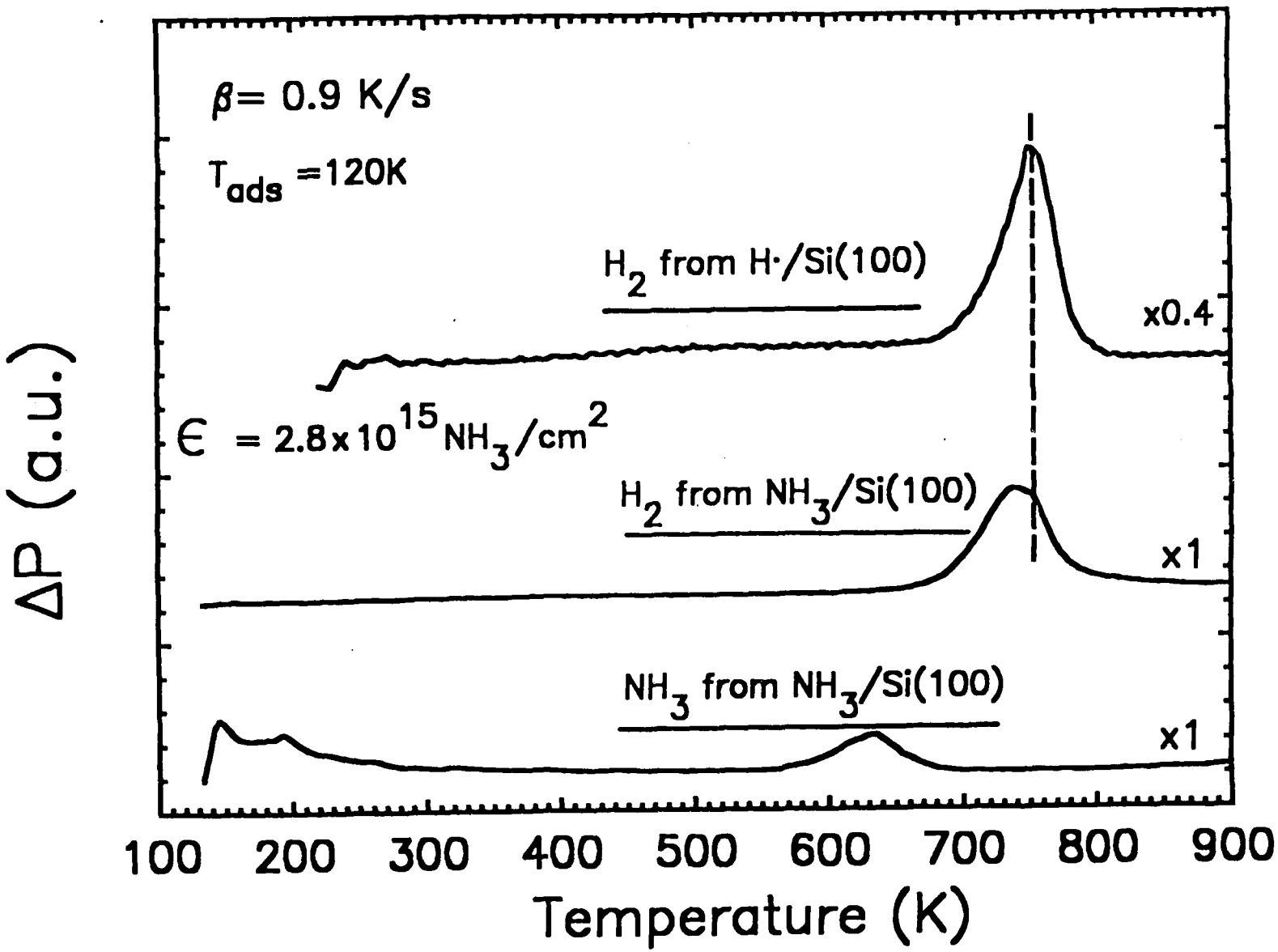

Dresser, Taylor, Wallace, Choyke, Yates

Figure 8

Deuterium Atom Coverage Calibration – Si(100)–(2x1)

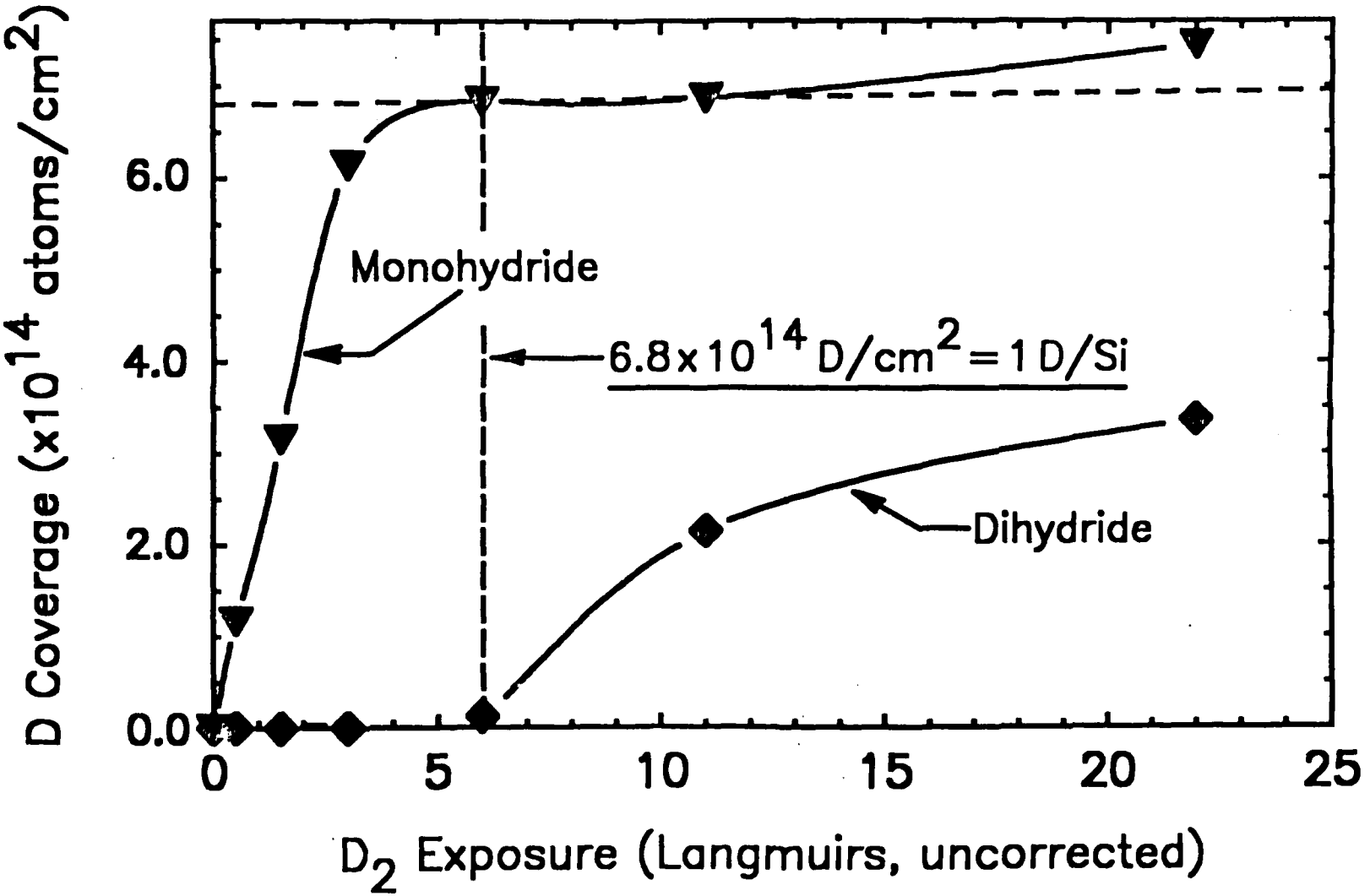

Dresser, Taylor, Wallace, Choyke, Yates

Figure 9

D–Atom Blockage of NH_3 Adsorption on Si(100)

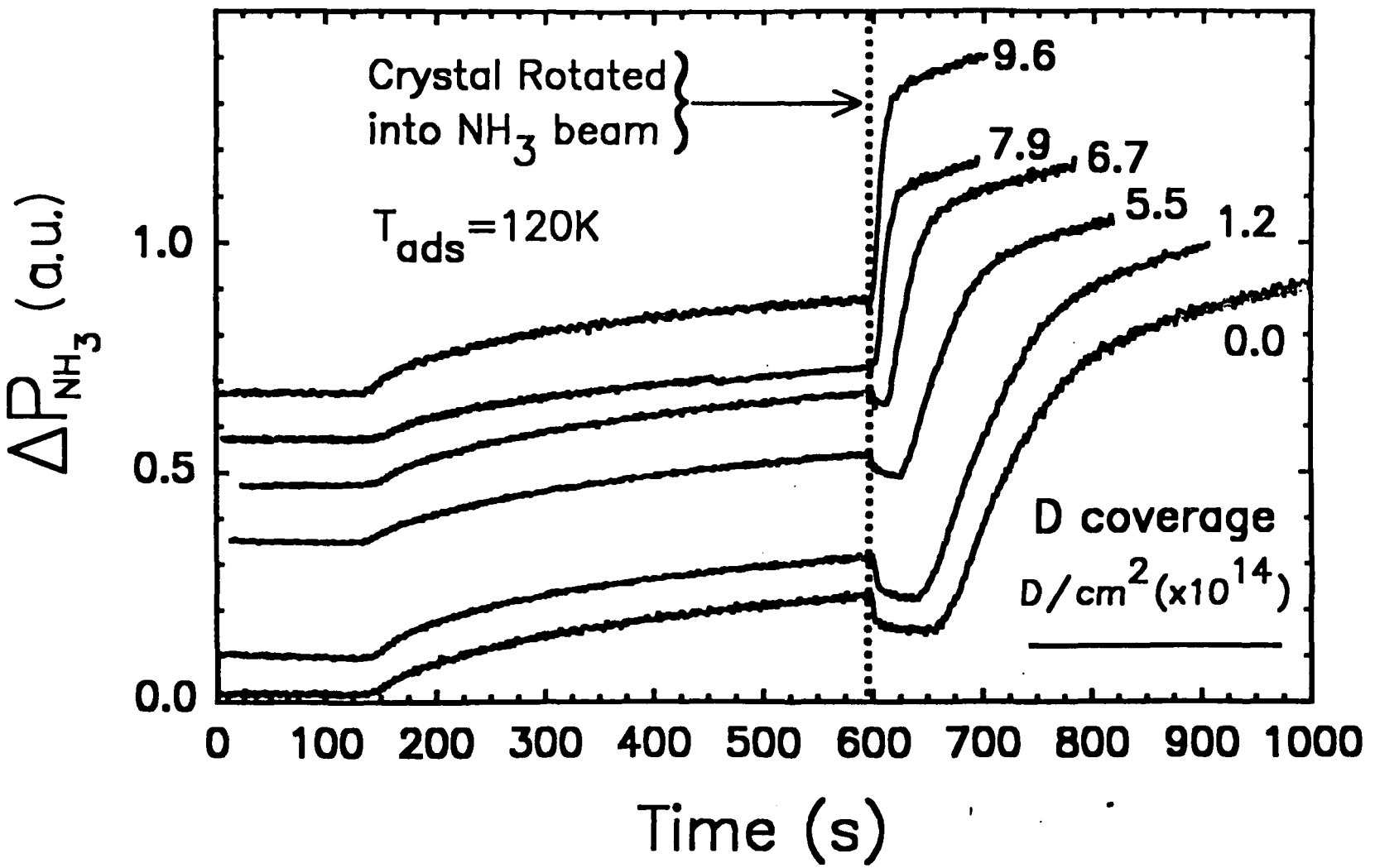

Dresser, Taylor, Wallace, Choyke, Yates
Figure 10

Distribution of Thermal Desorption Products from $NH_3/D\cdot/Si(100)$

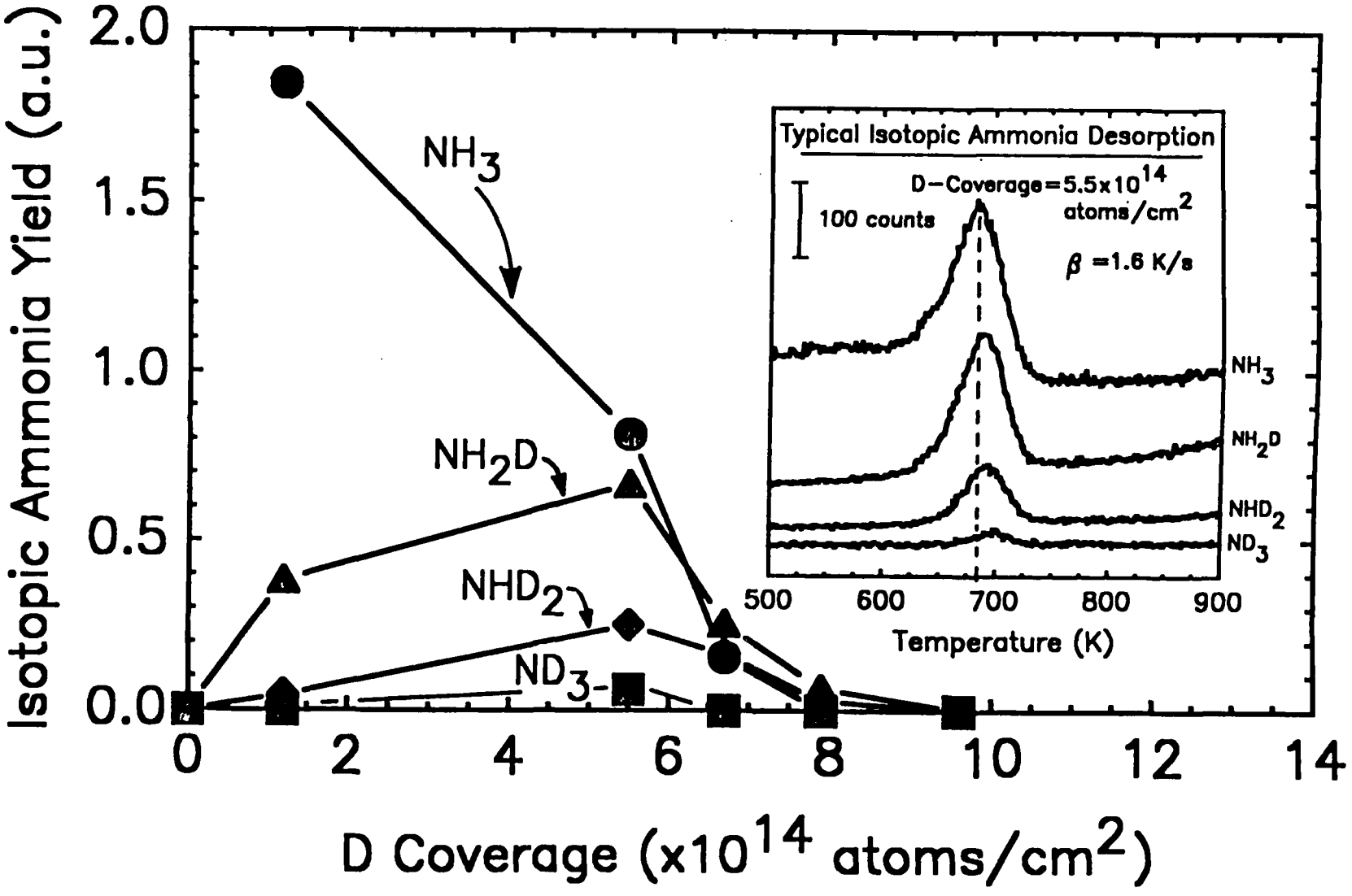

Dresser, Taylor, Wallace, Choyke, Yates
Figure 11

Auger Study of Nitrogen Behavior from NH_3/Si(100)

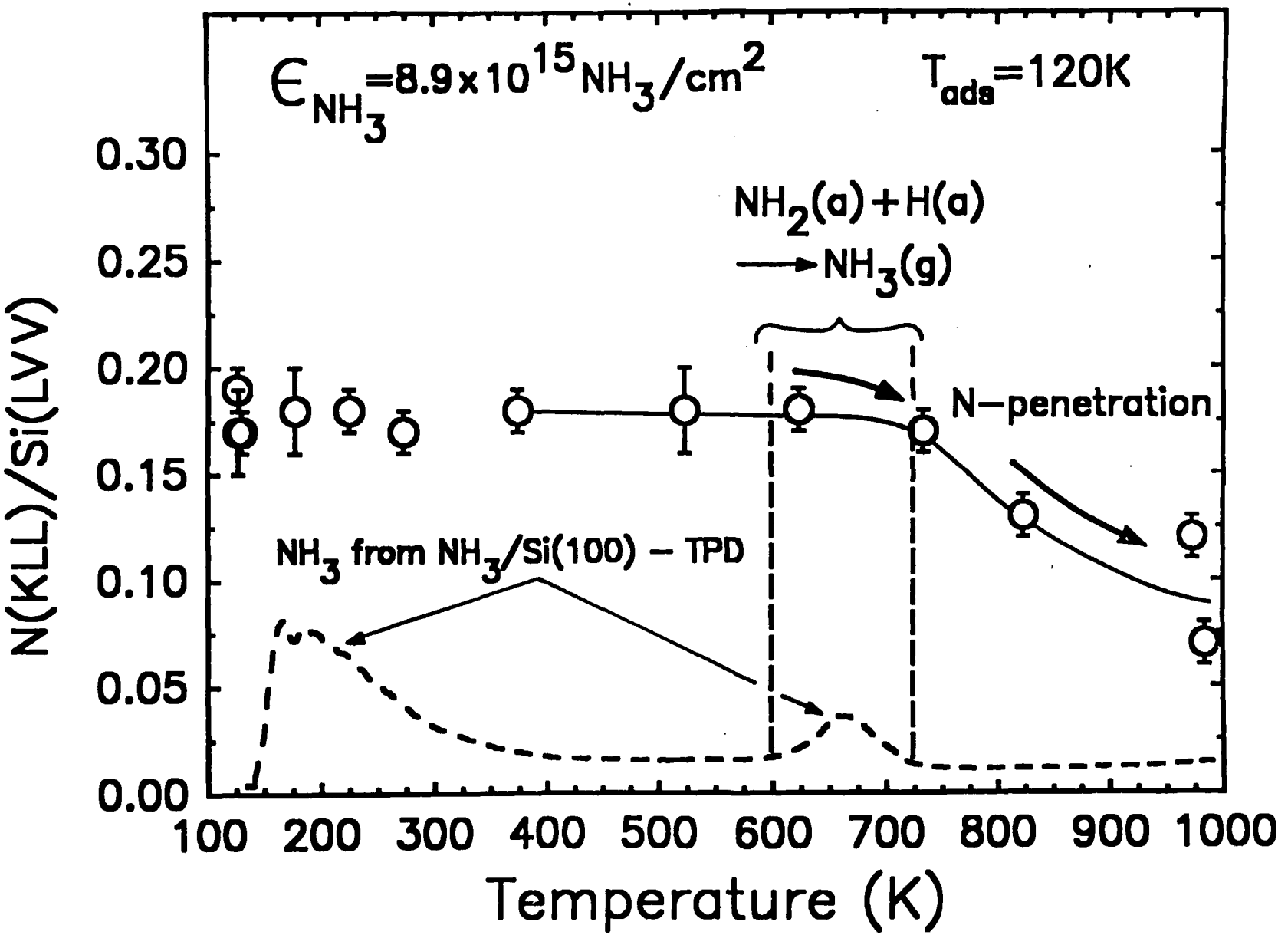

Dresser,
Taylor,
Wallace,
Choyke,
Yates
Figure 12

Relative Assay of Nitride Species from NH_3/Si(100)

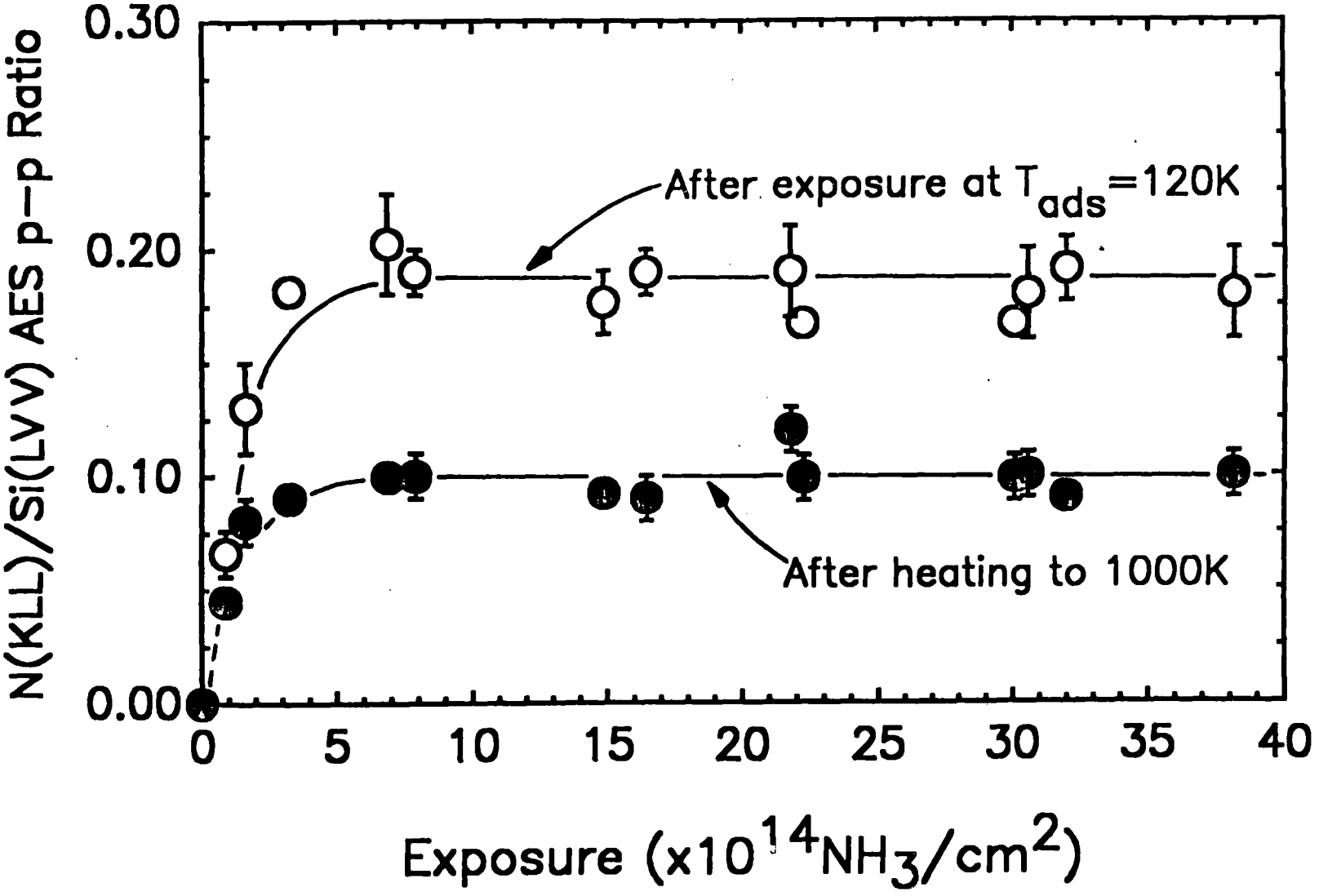

Dresser, Taylor, Wallace, Choyke, Yates

Figure 13

Digital LEED Patterns of Si(100)-(2×1)

E_p = 120 eV

Real Space Orientation

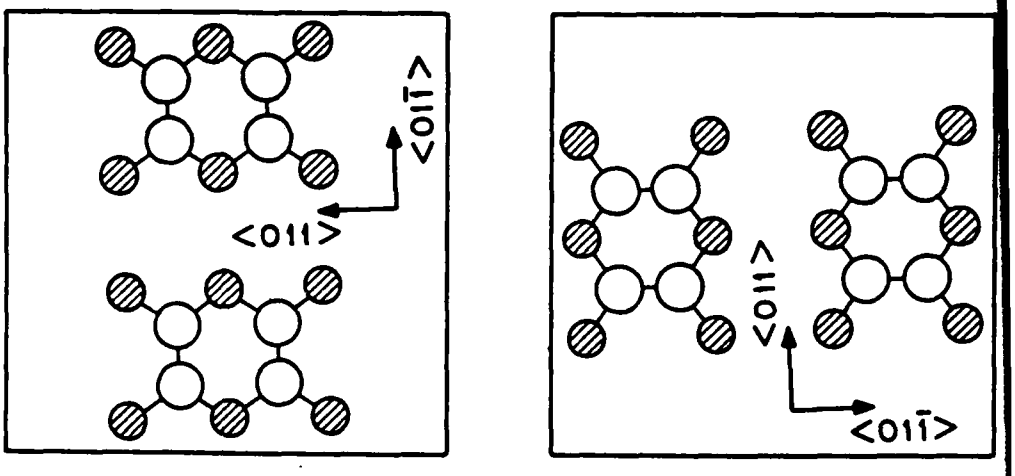

Corresponding LEED Patterns

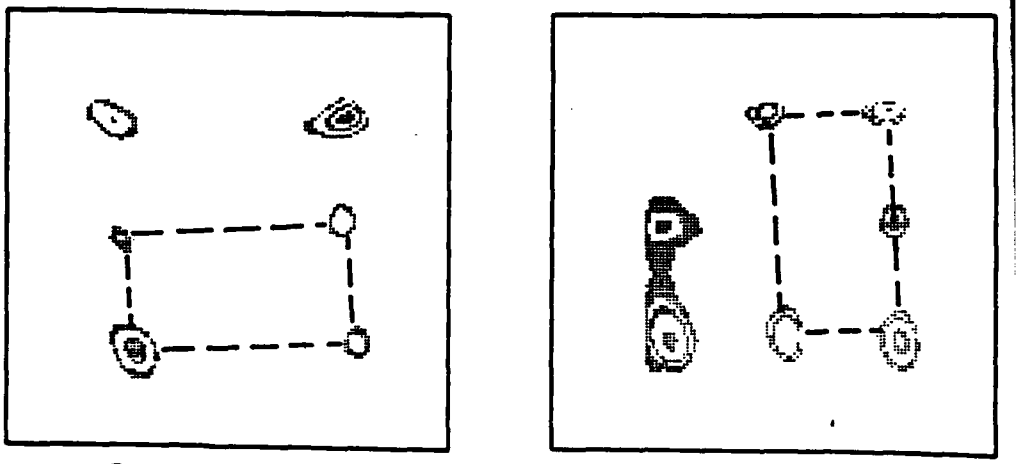

Orientation (a)

Orientation (b)

Dresser, Taylor, Wallace, Choyke, Yates
Figure 14

Two Fold Symmetric H^+ ESDIAD Patterns from $NH_3/Si($

$\epsilon = 2.1 \times 10^{14}$ NH_3/cm^2 $T = 115K$

a- Before crystal rotation

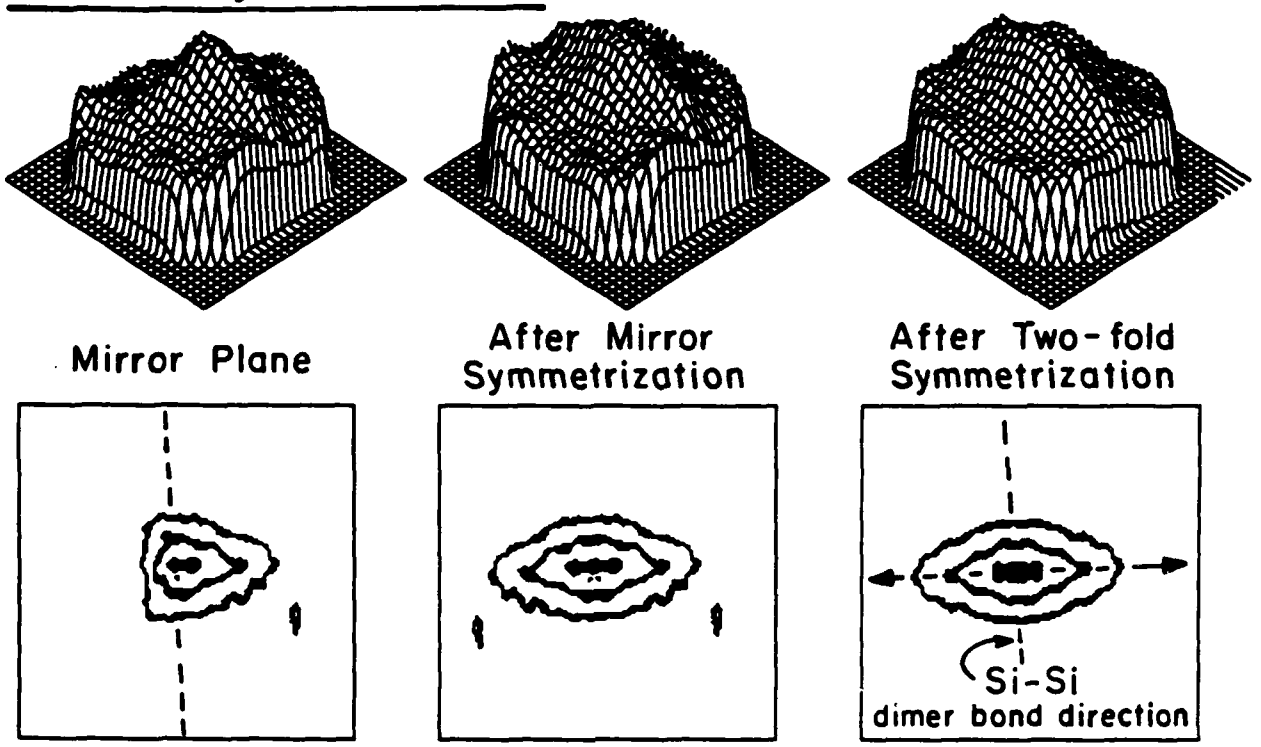

b- After crystal rotation

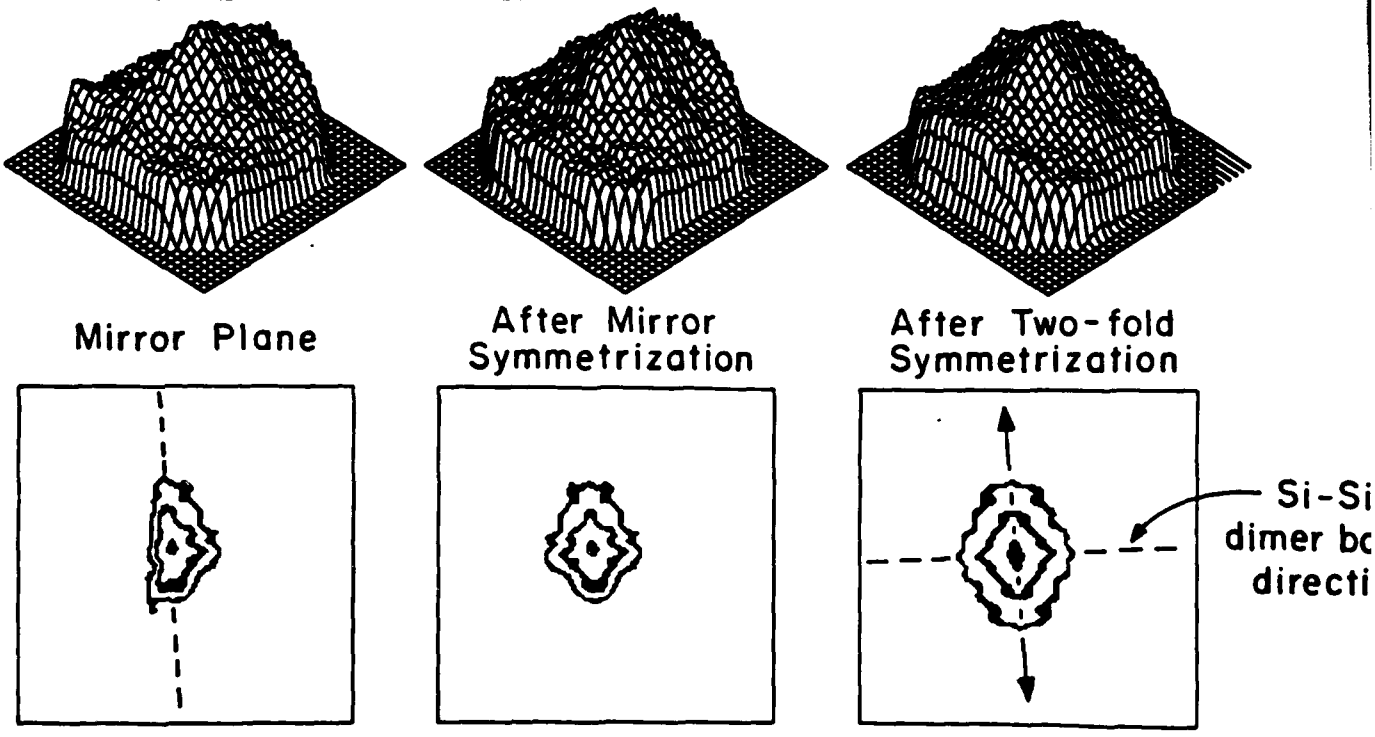

Dresser, Taylor, Wallace, Choyke, Yates
Figure 15

H^+ ESDIAD Patterns for Various NH_3 Exposures on Si(10

T=115K

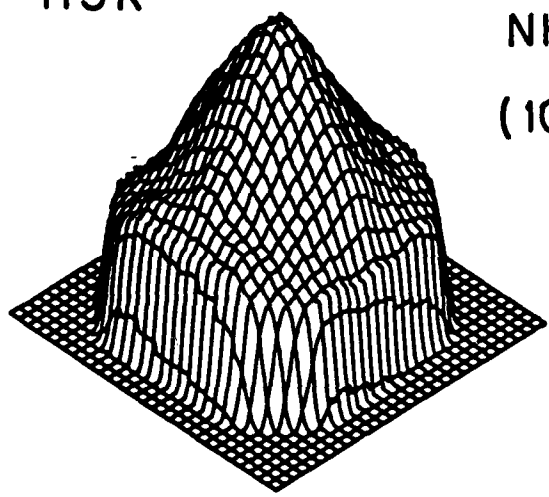

NH_3 Exposure
(10^{14} NH_3 cm^{-2})

11.1

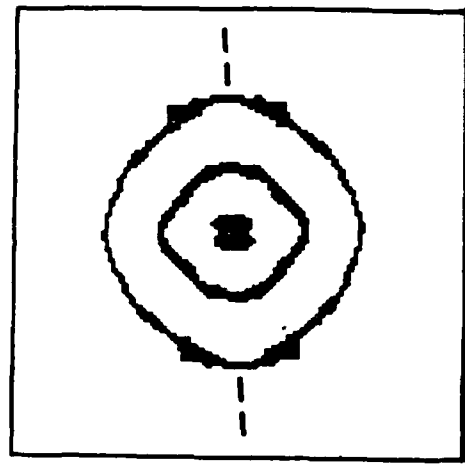

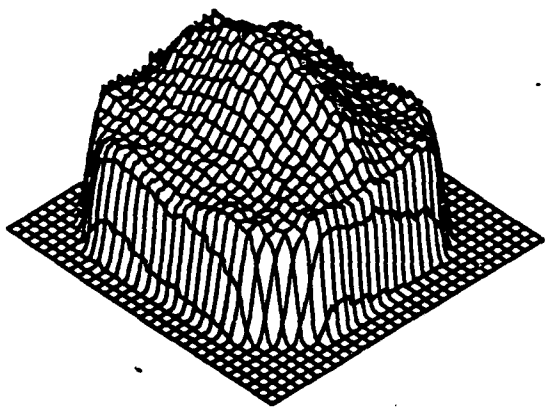

2.1

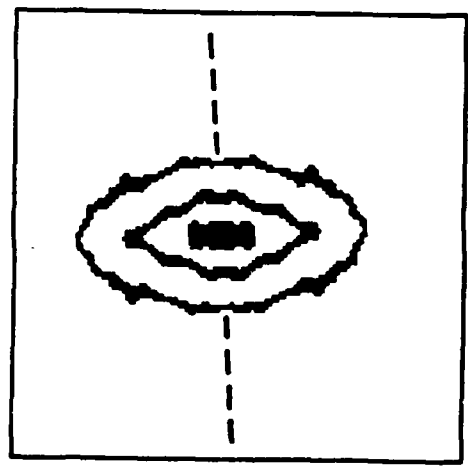

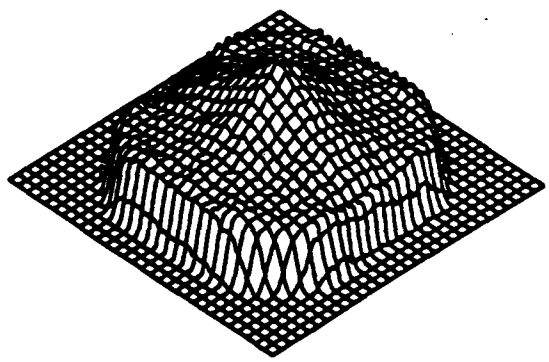

1.1

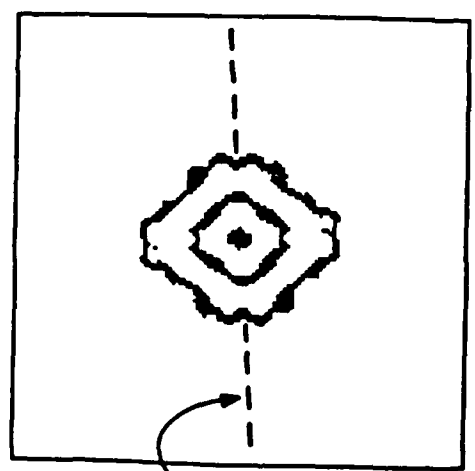

Si-Si
dimer bond
direction

Dresser, Taylor, Wallace, Choyke, Yates
Figure 16

H ESDIAD Pattern for Various Annealing Treatments of NH_3 on Si (100)

Exposure: 4.9×10^{14} NH_3/cm^2

$T_{max} = 130\,K$

Total H^+ Yield $= 1.2 \times 10^6$

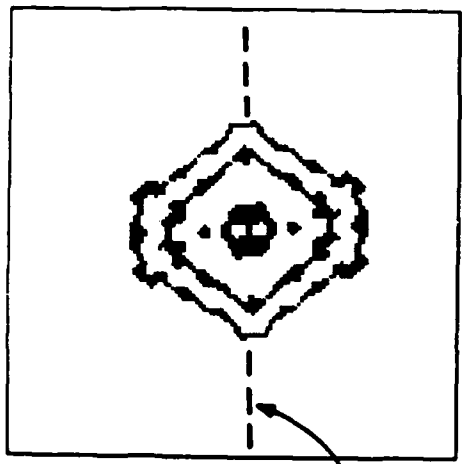

Si-Si dimer bond direction

$T_{max} = 183\,K$

Total H^+ Yield $= 0.7 \times 10^6$

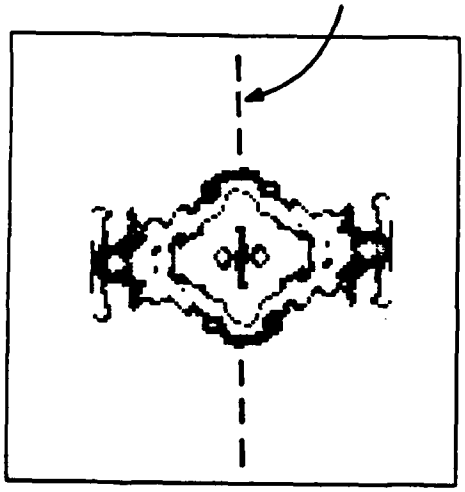

$T_{max} = 642\,K$

Total H^+ Yield $= 0.4 \times 10^6$

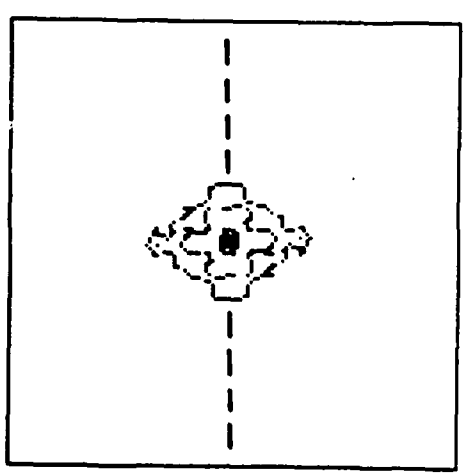

Dresser,
Taylor,
Wallace,
Choyke,
Yates
Figure 17

H^+ ESD–Yield as a function of Increasing Temperature NH_3 Adsorption on Si(100)

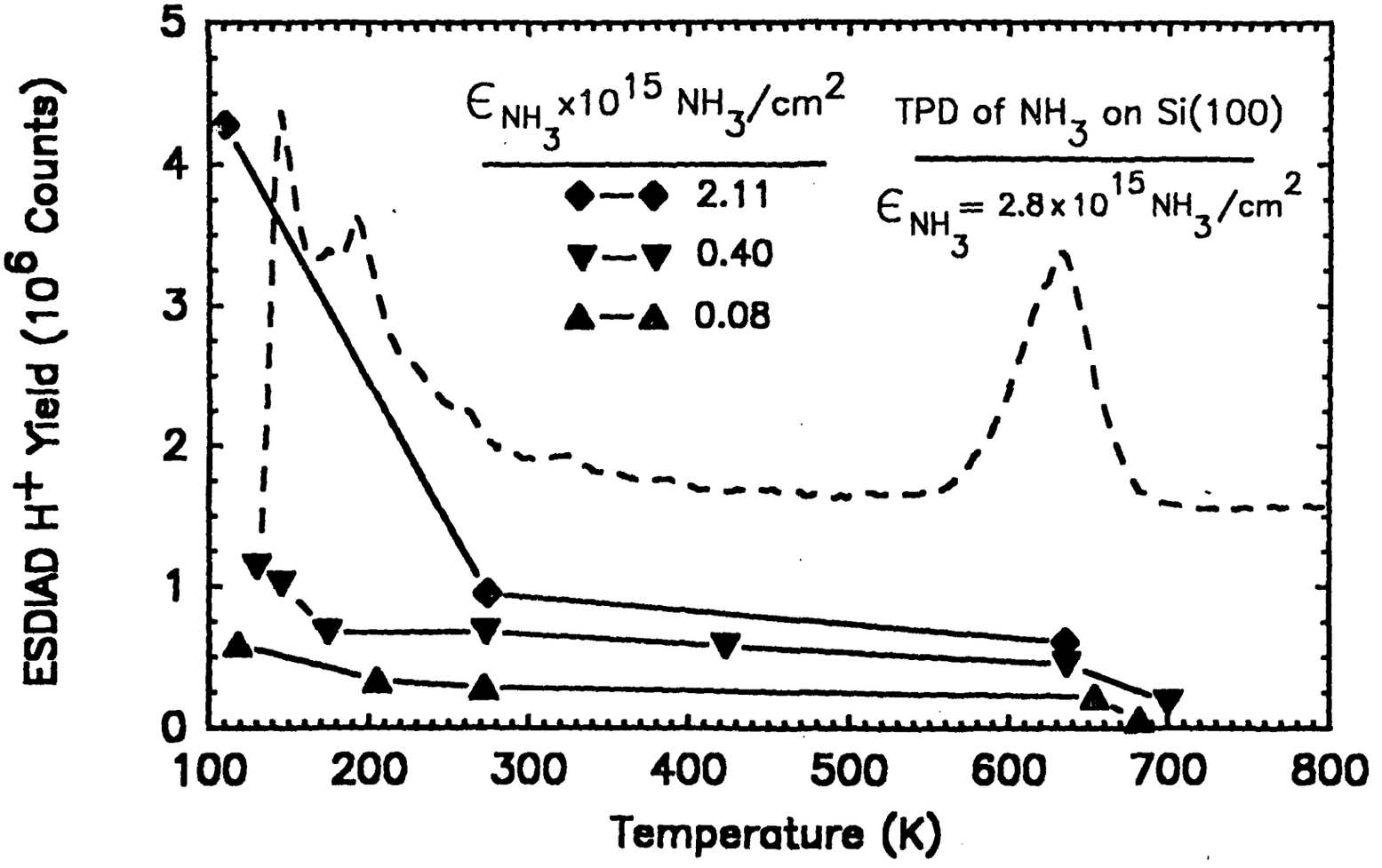

Dresser, Taylor, Wallace, Choyke, Yates
Figure 18

H^+ Ion Energy Distribution Following NH_3 Adsorption on Si(100)

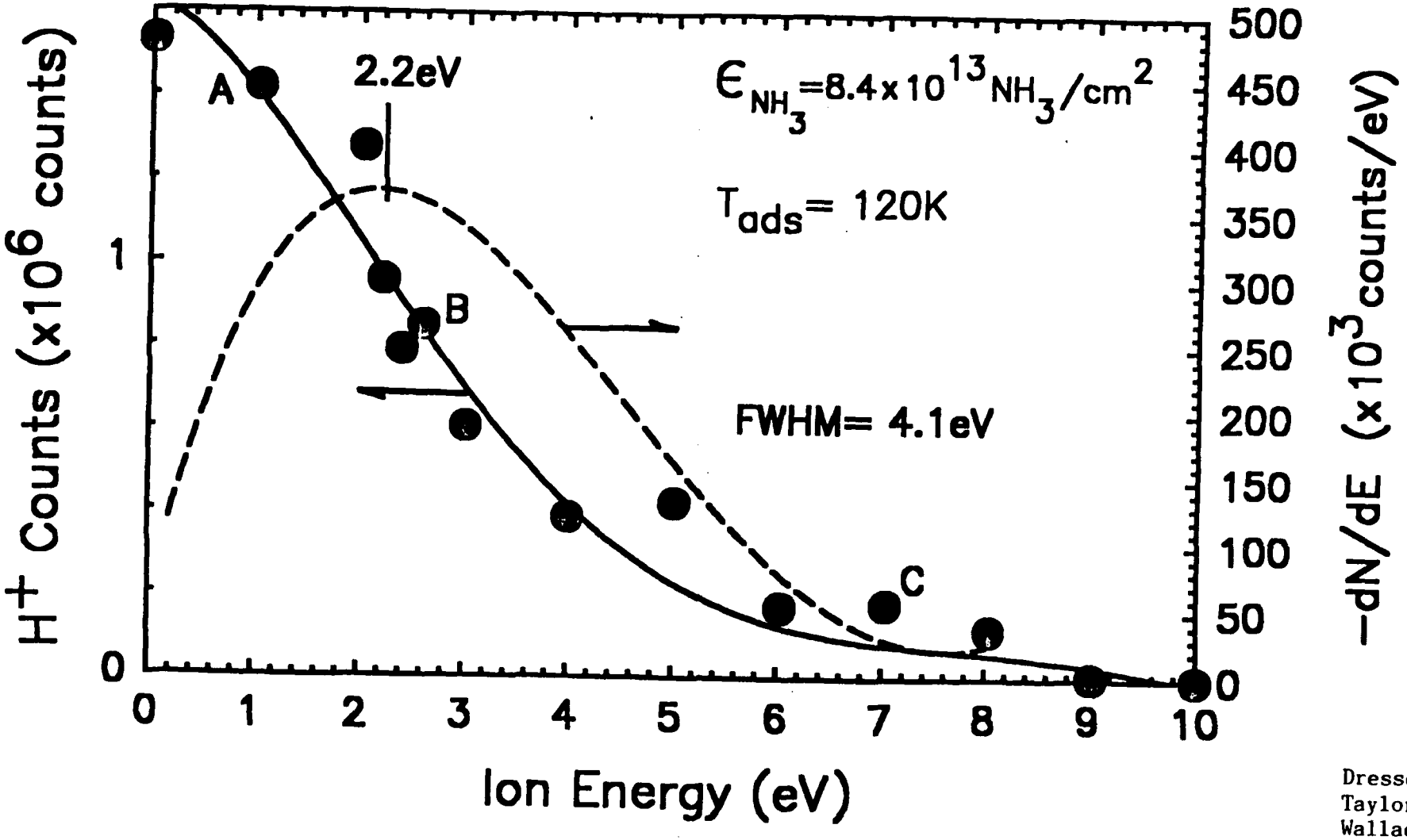

Dresser, Taylor, Wallace, Choyke, Yates
Figure 19

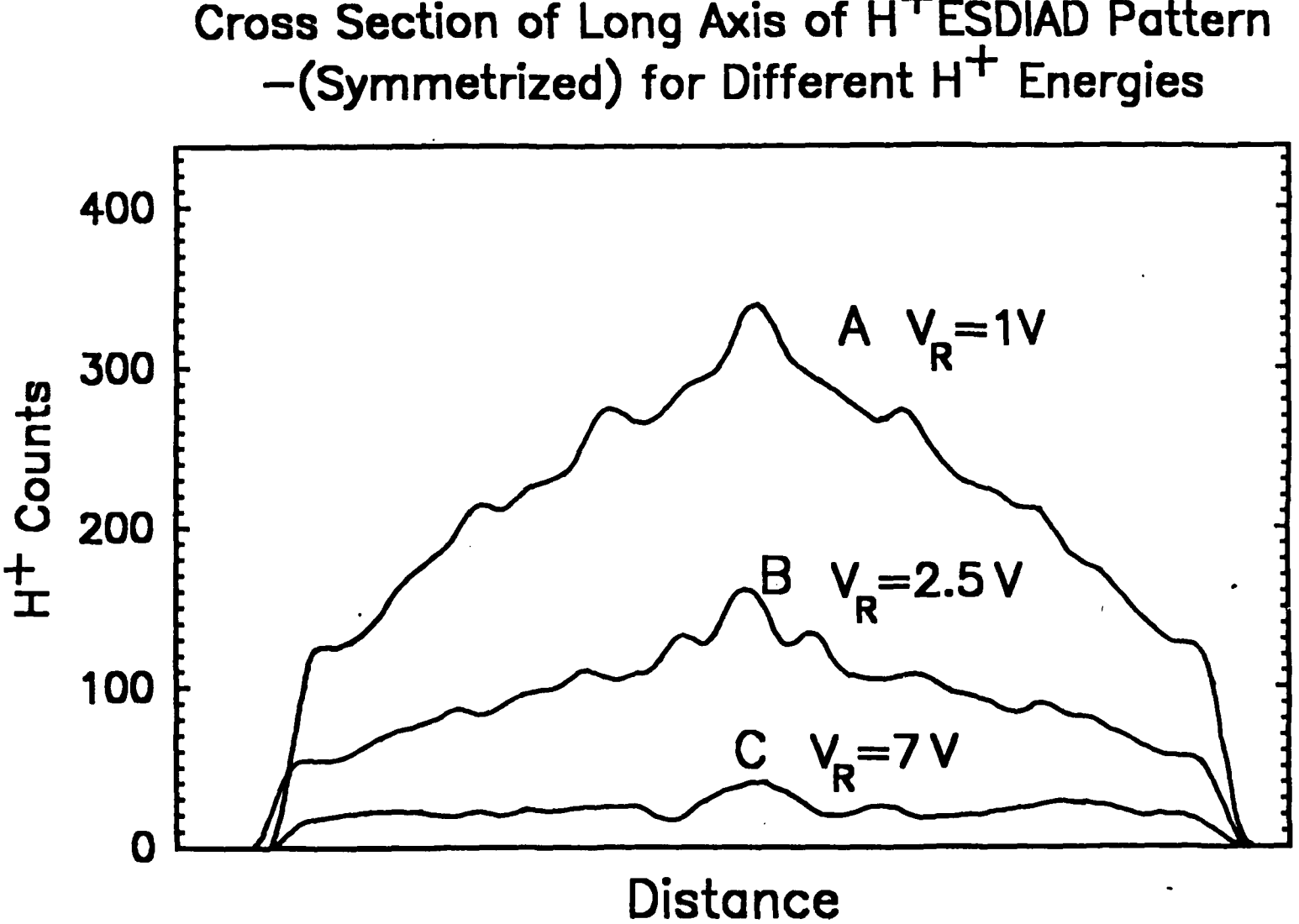

Dresser,
Taylor,
Wallace,
Choyke,
Yates
Figure 20

Schematic Geometry of NH_2 Species on Si(100)

Dimer Site

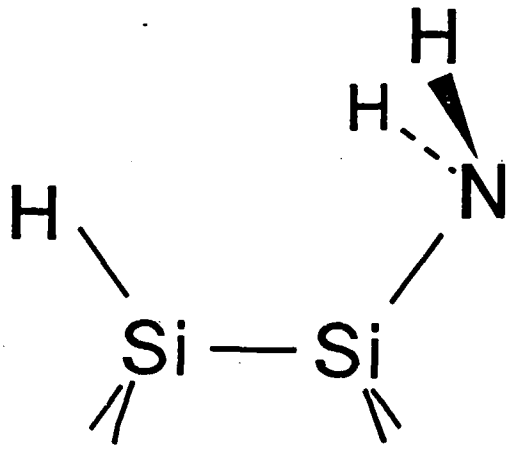

Dresser,
Taylor,
Wallace,
Choyke,
Yates
Figure 21

Torsional Motion of NH_2 /Si(100

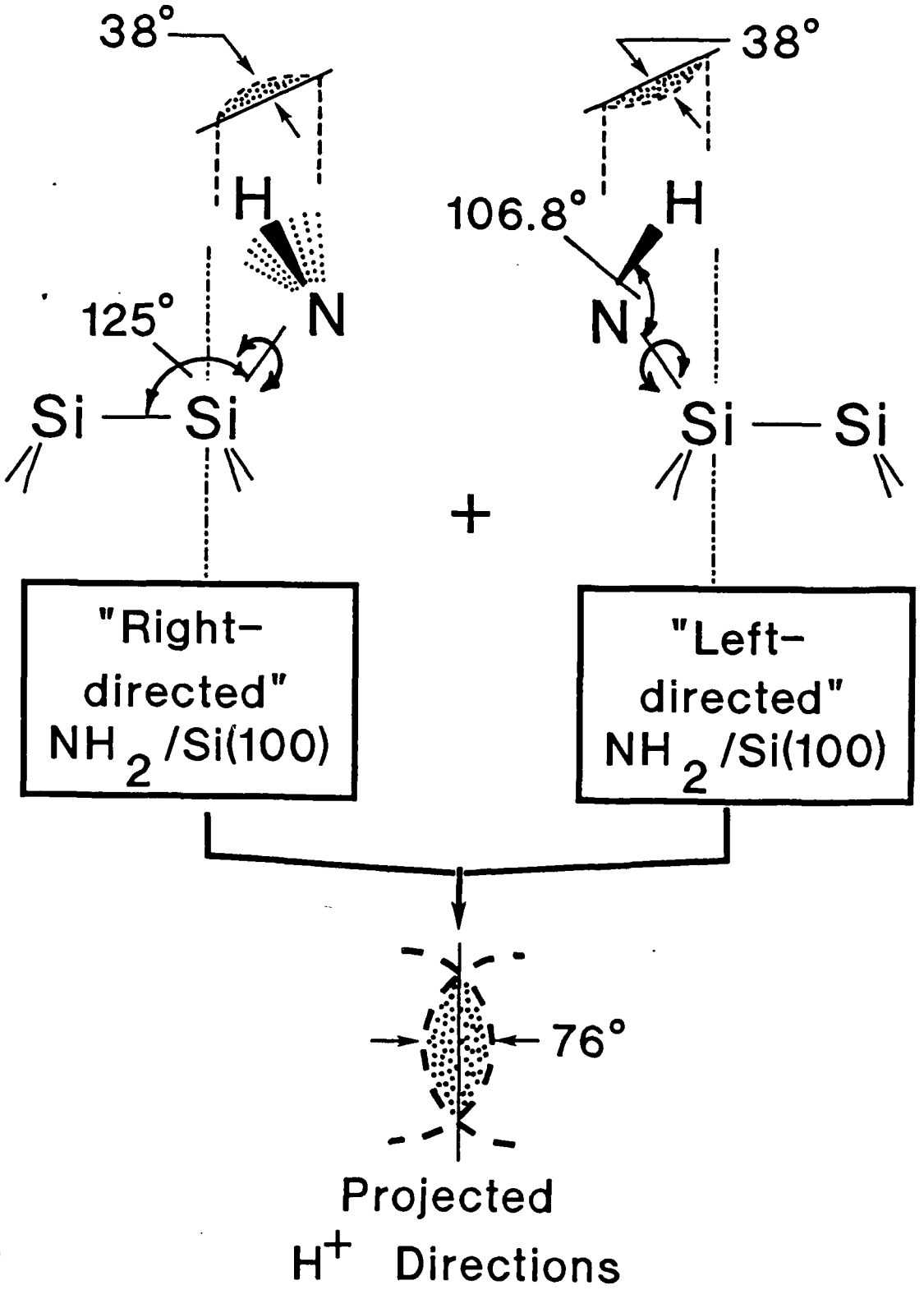

Dresser, Taylor, Wallace, Choyke, Yates
Figure 27

DL/413/83/01
GEN/413-2

TECHNICAL REPORT DISTRIBUTION LIST, GEN

	No. Copies
Office of Naval Research Attn: Code 413 800 N. Quincy Street Arlington, Virginia 22217	2
Dr. Bernard Douda Naval Weapons Support Center Code 5042 Crane, Indiana 47522	1
Commander, Naval Air Systems Command Attn: Code 310C (H. Rosenwasser) Washington, D.C. 20360	1
Naval Civil Engineering Laboratory Attn: Dr. R. W. Drisko Port Hueneme, California 93401	1
Defense Technical Information Center Building 5, Cameron Station Alexandria, Virginia 22314	13 ~~12~~
DTNSRDC Attn: Dr. G. Bosmajian Applied Chemistry Division Annapolis, Maryland 21401	1
Dr. William Tolles Superintendent Chemistry Division, Code 6100 Naval Research Laboratory Washington, D.C. 20375	1
Dr. David Young Code 334 NORDA NSTL, Mississippi 39529	1
Naval Weapons Center Attn: Dr. Ron Atkins Chemistry Division China Lake, California 93555	1
Scientific Advisor Commandant of the Marine Corps Code RD-1 Washington, D.C. 20380	1
U.S. Army Research Office Attn: CRD-AA-IP P.O. Box 12211 Research Triangle Park, NC 27709	1
Mr. John Boyle Materials Branch Naval Ship Engineering Center Philadelphia, Pennsylvania 19112	1
Naval Ocean Systems Center Attn: Dr. S. Yamamoto Marine Sciences Division San Diego, California 91232	1